RPAS-SfM Snow Depth and Snow Density Mapping in Disturbed Vegetated Mountainous Environments of Coastal British Columbia

By

Trevor Dickinson

BA Double Major in Physical Geography and First Nations Studies

Vancouver Island University, 2018

A Thesis Submitted in Partial Fulfillment of the Requirements for the Degree of

MASTER OF SCIENCE

In the Department of Geography

RPAS-SfM Snow Depth and Snow Density Mapping in Disturbed Vegetated Mountainous Environments of Coastal British Columbia

By

Trevor Dickinson

BA Double Major in Physical Geography and First Nations Studies

Vancouver Island University, 2018

Supervisory Committee

Dr. Randel Scharien, Co-Supervisor
Department of Geography

Dr. William Floyd, Co-Supervisor
Department of Geography

Abstract

Concurrent advancements in Remotely Piloted Aircraft Systems (RPAS) and Structure from Motion (SfM) processing technologies have added powerful new methods for remotely sensing the cryosphere. Highly accurate snow depth (SD) estimates derived from RPAS-SfM workflows have been attained, however, most studies have examined open, relatively simple terrain. Results from the few RPAS-SfM SD studies that have examined complex vegetated terrain are of insufficient accuracy for meaningful use in water-resource research and management, prompting further development of RPAS-SfM SD and snow water equivalent (SWE) survey methods to better represent such areas. This study researched the use of RPAS-SfM methods to map SD and SWE across a 52 hectare study plot located on Vancouver Island, British Columbia during two snow seasons. This mid-elevation plot contains steep and complex terrain, including roads, ground covering perennial shrubs, regenerating forest, and old-growth forest. Optical imagery was captured using an off-the-shelf RPAS, and processed into digital elevation models (DEMs) using SfM software. Bare earth DEMs were then subtracted from snow surface DEMs to derive SD estimates. Manual SD measurements were used to validate RPAS-SfM SD estimates, and manual SWE measurements were used to estimate SWE across the study area. Additionally, the efficiency and accuracy of a novel, permanent above snow Ground Control Point (GCP) network was assessed. Root mean square error (RMSE) as low as 0.08 m was found in open terrain, which is consistent with previous research. In off-road areas, RMSE initially ranged from 0.36 m to 0.59 m, however, a bias correction based on ground cover classifications was found to be effective for dealing with underestimations of SD values caused by thick perennial vegetation; with vegetation caused bias ranging from -0.25 m to -0.46 m the application of a positive offsets reduced RMSE by up to 0.27 m in off-road sections, resulting in best case RMSE of 0.18 m in such areas. Multi-temporal SD and SWE outputs captured peak and melt period snowpack conditions, presenting highly detailed information on snow distribution, melt dynamics, and total stored water across the study plot. The elevated permanent GCP network was found to greatly improve the efficiency of both field surveys and data processing, while providing sub-centimeter accuracy levels similar to traditional ground level GCPs. Methods developed through this research show that RPAS-SfM techniques can be successfully applied to previously logged areas containing ground covering vegetation, and offer promise for application in water management of such areas.

Keywords

Snow depth, snow water equivalent, remote sensing, remotely piloted aircraft systems, Structure from Motion, digital terrain modelling, water management, hydrology, forestry

Table of Contents

List of Tables

List of Figures

List of Acronyms

CHRL- Coastal Hydrology Research Lab

DEM- Digital Elevation Model

GCP- Ground Control Point

GNSS- Global Navigation Satellite System

GSD- Ground Sampling Distance

LiDAR- Light Detection and Ranging

MAE- Mean Absolute Error

MRE- Mean Relative Error

NIR- Near Infrared Reflectance

NRCAN- Natural Resources Canada

RCEW- Russell Creek Experimental Watershed

RMSE- Root Mean Square Error

RPAS- Remotely Piloted Aircraft Systems

RTK- Real Time Kinetic

PDOP- Position Dilution of Precision

SD- Snow Depth

SfM- Structure from Motion

SWE- Snow Water Equivalent

UAV- Unmanned Aerial Vehicle

Acknowledgements

This thesis research project has been an exciting and challenging journey that was made possible by the incredible guidance and encouragement of many wonderful people around me. I never thought I would go to university, let alone complete a MSc, but here I am! Fieldwork for this project was at times very challenging, but also a lot of fun. Thank you to the amazing individuals who joined me at Russell Creek throughout the two field campaigns, including volunteers Chloe Sandahl, and Kyle Sharpe, and my amazing lab mates Stewart Butler, Ali Bishop, Alexander Cebulski, and Tomas Kulaja; a special thanks goes to Griffin Fisk for your collecting of many hundreds of manual snow measurements, your RTK GNSS expertise, and getting many sleds unstuck, too. I would like to thank my parents, Barbra Wilson and Rene Antonissen for teaching me the importance of hard work, and for encouraging me throughout my academic journey. To my supervisors Dr. Bill Floyd and Dr. Randy Scharien, thank for your guidance, and very importantly, your patience throughout the last 2.5 years. I knew that doing a MSc would be a major challenge, and I am forever grateful for all the hard work you both put in to making sure I got across the finish line. Finally, I would like thank to my wife, Hannah Hall. Without you, this journey would have never begun. Your endless encouragement, support, and care was critical to my success throughout both my BA, and my MSc. I am proud of how far I have come, and to be a first generation post-secondary student, and without you all, I would not have made it to this point. Thank you

Chapter 1 Introduction

1.0 Introduction

Obtaining accurate and timely snowpack data is critical to flood and water supply forecasting around the world (Harder et al., 2016; Nolan et al., 2015). A variety of data collection methods with varying strengths and weaknesses are used by decision makers to monitor snowpack levels, including automated weather stations, manual snow course surveys, crewed aerial LiDAR and photographic surveys, and satellite-based sensors. Automated weather stations produce accurate data at point locations using such methods, however, the heterogeneity of snow depth across a landscape is poorly represented (Nolan et al., 2015). Manual snow surveys provide good measurement data across wider areas of 100 – 1000's m^2 compared to the small footprint of a few m^2 that a weather station covers, but in addition to being spatially restricted, they are labour intensive (Harder et al., 2016; Nolan et al., 2015). Crewed aerial LiDAR and photographic surveys can provide highly detailed information over large areas, however, costs can be prohibitive, and weather can delay timely data collection (Deems et al., 2013). In addition to being temporally restricted and weather dependent, to date, satellite remote sensing is unable to provide snow depth (SD) measurements at levels of accuracy adequate for water management purposes in complex terrain, or areas containing shallow snowpack (Marti et al., 2016) .

The concurrent advancements of Structure from Motion (SfM) photogrammetry and Remotely Piloted Aircraft Systems (RPAS) technologies have made it possible to conduct highly accurate, spatially broad, on-demand landscape change detection surveys, at a reasonable cost

(Colomina & Molina, 2014; Whitehead & Hugenholtz, 2014). SfM photogrammetry creates 3D models through a process of matching of points within overlapping images (Westoby et al., 2012). SfM scenes are transformed to real world coordinate systems with elevations by tying-in ground control points (GCPs); GCPs consist of static objects visible in captured images or set out targets with known, high precision, coordinates. Many excellent examples of innovative landscape change detection studies from RPAS-SfM exist, including research of landslides (eg. Fernández et al., 2016; Izumida et al.,2017; Lucieer et al., 2014), vegetation distribution and characteristics (Cunliffe et al., 2016), and tree growth (Guerra-Hernández et al., 2017). As noted in Bühler et al. (2016), prior to modern technological advancements, early examples of digital photogrammetric snow mapping from air photos existed, however, low accuracy levels of ~ 1.25 m limited meaningful SD estimates from being obtained (Cline, 1993). The use of modern RPAS-SfM techniques to study the cryosphere date back to at least 2012, when Solbø and Storvold (2013) combined RPAS mounted laser altimetry and optical imagery to measure the mass of a remote glacier in Svalbard. The first strictly RPAS-SfM survey of a glacier was conducted by Ryan et al. (2015). Also in 2015, the first RPAS-SfM photogrammetry study measuring SD was published (Jagt et al., 2015). In recent years several more studies have been published, with RPAS-derived SD root-mean-square error (RMSE) of <10 cm regularly reported (Avanzi et al., 2018; Bühler et al., 2016; Bühleret al., 2017; Cimoli et al., 2017; Harder et al., 2016; Revuelto et al., 2021). Common in all of these papers is the study of primarily open and topographically-simple terrain.

Lendzioch et al. (2016) and Miziński and Niedzielski (2017) pioneered the use of RPAS-SfM to measure SD in forested areas, however, results contained relative error greater than

100%. Harder et al., (2020) further explored the use of RPAS-SfM for estimating SD in a forested area, while also comparing it to RPAS mounted LiDAR; they determined that RPAS-SfM methods are not useful for mapping SD under forest canopy, but reaffirmed their utility in open areas.

In the Pacific Northwest region of North America where this study took place, forests are the dominant land cover type. The region is characterized by high precipitation levels throughout the fall, winter, and spring months, with deep seasonal snowpack common in mountainous areas. Natural and human caused disturbances are widespread in this region, which can alter snow hydrology. Snow accumulation and melt is greatly altered in clear cuts (eg. Jost, Weiler, Gluns, & Alila, 2007), as well as areas impacted by forest fires (e.g. Vore et al., 2020), which have burned on average 348,917 hectares annually between 2011 and 2020 in BC (Province of British Columbia, n.d.). In these disturbed areas, generally more snow accumulates than in mature forest because less, or no, canopy interception occurs. With increased exposure to radiative and latent heat fluxes in harvested or burned areas, snow melt generally occurs at a faster rate than in forested stands, which can increase and alter the timing of peak stream flow rates in effected watersheds (eg Jost et al., 2007; Vore et al., 2020). With wide-scale logging continuing across the region, and forest fire severity and total area burned increasing due to climate change, the ability to monitor snow in such disturbed areas has never been more important (Vore et al., 2020).

Forested regions in BC and around the world hold important water resources in the form of snow. The ability to use RPAS-SfM technologies to measure SD and variations of snow distribution across different terrain and elevation bands in disturbed, vegetated, and

topographically complex areas adds an important new tool that can measure snow with increased resolution and accuracy. However, methods must be developed to measure and assess uncertainty in these environments, while also addressing high error values that have been found in RPAS-SfM outputs examining such terrain (Harder et al., 2020; Harder et al., 2016; Jagt et al., 2015).

This thesis research combines recent RPAS-SfM SD survey methods with novel approaches to improve the ability to map SD in disturbed complex vegetated mountain environments. Also developed are methods to estimate SWE and total stored water from SD DEMs for use in operational settings such as water resource management. By improving RPAS-SfM methods for use in complex vegetated landscapes, including harvested and disturbed areas, the ability to accurately monitor hydrological processes and evaluate impacts of landscape changes from economic activities in mountainous coastal watersheds can be enhanced. To date, the use of RPAS-SfM methods to measure SD in regenerating forests with complex ground cover has not been attempted, and doing-so will add to a growing body of SfM literature assessing methodology and uncertainly across a variety of terrain types. Benefits of this research include expanding the utility of a tool that can be used by researchers and decision makers to monitor SD change, forecast floods, manage water supplies, and assess seasonal variability (short term) and climate change (long term). Further, methods developed here can be utilized to monitor the hydrological and ecological impacts of both industrial disturbances such as logging, and natural disturbances such as forest fires at both the stand level, and downstream. RPAS-SfM SD measurement techniques can also be combined with plane-based LiDAR snow surveying outputs to extrapolate RPAS derived SD estimates across much greater areas (Broxton & van Leeuwen,

2020). Beyond SD mapping, this research stands to contribute to the advancement of RPAS snow detection techniques and landscape change detection capabilities within the geosciences in general. Combined with existing snow monitoring methods such as automated weather stations, snow courses, and contemporary plane-based LiDAR surveying, enhancements to RPAS – SfM methods will expand our ability to assess seasonal SD.

1.1 Research Questions and Objectives

A workflow was developed to map SD and SWE in complex, disturbed mountainous coastal environments. Modifications were applied to existing SD and SWE survey and data processing methods to improve results in the disturbed, vegetated, complex terrain examined. Novel georeferencing methods were used to improve efficiency and accuracy levels as described below.

Specifically, the following questions were addressed:

1) How can optical imagery from RPAS be used to accurately map SD in disturbed, complex, vegetated terrain?
2) How can representative SWE be estimated for disturbed, complex, vegetated terrain using RPAS derived SD digital elevation models?

1.2 Thesis Structure

This thesis is formatted into five chapters; Chapter 2 consists of a literature review, including the fundamentals of SfM photogrammetry, LiDAR based SD and SWE research, and a variety of RPAS-derived terrain differencing studies, including SD based studies. Chapter 3

presents the study area and methods. Chapter 4 presents the results and discussion, while Chapter 5 provides a conclusion of this project, including recommendations for future research.

Chapter 2.0 Literature Review

The development of RPAS technology has introduced a low cost means of remotely sensing the Earth's surface at significantly increased temporal and spatial scales compared to traditional plot-based methods. Within the short history of contemporary RPAS based landscape surveying, many examples exist of researchers using these new technologies to better describe variation and landscape characterises, e.g. landform change detection (Lucieer et al., 2014), natural disaster mapping (Izumida et al., 2017), wildlife population enumeration, construction site surveying, and much more (Gaffey & Bhardwaj, 2020; Whitehead & Hugenholtz, 2014) . Within the Geosciences, RPAS use has become widespread (Gaffey & Bhardwaj, 2020; Giordan et al., 2018; Whitehead & Hugenholtz, 2014). No longer needing to rely on satellite and crewed aircraft based remote sensing, geoscientists now have the ability to monitor surface processes at a near on-demand basis with greater flexibility, at much lower costs (Hugenholtz et al., 2013; Izumida et al., 2017; Lucieer et al., 2014; Whitehead & Hugenholtz, 2014). Much of the interest in RPAS technology is rooted in the concurrent development of user-friendly SfM software such as *Agisoft PhotoScan* and *Pix4D*, which allows images captured from purpose-made consumer and professional grade RPAS to be processed into high resolution georeferenced digital elevation models (DEM) and orthophotographs (Colomina & Molina, 2014; Whitehead & Hugenholtz, 2014). Through creation of sequential DEMs that are spatially co-registered, change detection analysis can be applied to measure a variety of landscape processes at high temporal and spatial resolution (e.g. Colomina & Molina, 2014; Whitehead & Hugenholtz, 2014).

Ground Sampling Distance (GSD) dictates the representative pixel size, and is determined by the resolution of the camera and the elevation of the RPAS during acquisition (Colomina & Molina, 2014). To produce DEMs with consistent resolution, images must be collected at a steady altitude over the surface. Because of the inherent low contrast nature of snow surfaces, RPAS surveys need to be flown at relatively low altitudes to return point matching levels that will produce DEMs with high resolution and accuracy. The majority of previous studies have conducted RPAS flight in the vicinity of 50 – 100 m above the surface, which typically produces a GSD in the range of 2 – 5 cm (Gaffey & Bhardwaj, 2020; Revuelto, Alonso-Gonzalez, et al., 2021).

Ground control points are required to georeference RPAS derived DEMs (Gindraux et al., 2017). Locations of GCPs are typically recorded in the field using Real Time Kinetic (RTK) Global Navigation Satellite System (GNSS) units, which are capable of sub-centimetre precision, and later incorporated into DEM processing (Gindraux et al., 2017). The high accuracy of RTK GNSS is attained through the use of either permanent reference stations, or base stations set up by users to collect and average GNSS coordinates over a multi-hour collection period. Coordinates are then applied as corrections to rover units that field crews use to collect coordinates at GCPs, and in the case of SD surveying, typically also at locations where snow measurements are collected for validation purposes (Donahue et al., 2013).

Agisoft Photoscan and *Pix4d* photogrammetry software are the primary software packages being utilized within the existing literature (Gaffey & Bhardwaj, 2020). Image and coordinate data are imported into a SfM photogrammetry software where they are processed into point clouds and DEMs (Whitehead et al., 2014). Photos are first aligned using coordinates

attached to RPAS images, and then processed into dense point clouds using RTK GNSS GCP coordinates, providing the georeferencing accuracy and precision necessary for change detection analysis. DEMs and orthophotographs in snow surveying, snow surface and bare earth DEMs are normally created and used to estimate SD, simply by subtracting the bare earth DEM from the snow surface DEM. For accuracy assessments, georeferenced manually measured SD validation points are normally imported into the SD model for comparison with RPAS - SfM outputs (Gaffey & Bhardwaj, 2020).

2.1 SD RPAS SfM

In 2015, the first peer-reviewed English language publication on the use of RPAS-based SfM photogrammetry to estimate and map SD was published (Jagt et al., 2015). In that study, they examined a 0.007 km^2 plot in a mountainous area of Tasmania where ground cover consisted of thick shrubs with sparsely spaced trees. During their single snow survey field visit, a SD range of 0.33 – 1.21 m and mean SD of 0.62 m (standard deviation 0.24 m) was found from manual measurements. Utilizing a custom-built multi-rotor RPAS, a SD estimation RMSE of 0.096 m was achieved, with manual measurements consistently showing a negative bias in the RPAS-SfM model. They found that error values were greater in low SD locations; a relative error of 27.6% was found where SD was ~ 0.35 m; relative error was reduced to 8% in areas with SD of ~ 1.2 m. A total of 31 GCPs were distributed throughout the study area, with coordinates recorded using a dual-frequency differential GNSS unit. To validate SD, the same GNSS unit was used to collect coordinates with the base of the survey pole positioned at the snow surface, before plunging it through the snowpack to the ground to collect another coordinate. Problems were encountered with this technique in locations where undetected

vegetation under the snowpack introduced measurement errors, while potential for additional error exist in the form of coordinate errors; no other examples of this validation procedure are found within the existing literature. As part of this study, additional DEM processing was done to test how RMSE is affected by the absence of GCPs; without GCPs, RMSE increased from 0.096 m to 0.184 m, however, because the area surveyed contained features that were visible in both snow and bare earth surveys, an affine transformation was able to be used, reducing the non-GCP DEM RMSE to 0.08 m.

During the winter of 2013/14, De Michele et al. (2016) conducted a single snow survey of a 0.3 km^2 gently sloped, grass and rock covered terrain in the Italian Alps. Due to wind transported snow filling depressions in the landscape, SD varied considerably; gullies and stream beds had SD as high as 4.40 m, while some features in the landscape were almost snow free. A fixed wing RPAS was flown ~ 130 m above the ground, capturing images with 80% image overlap. A minimum of 13 GCPs were randomly distributed throughout the study area during each survey, while avalanche probes were used to collect 12 manual SD measurements at random individual locations. When compared to manual measurements, RPAS SD estimates resulted in a RMSE of 0.143 m; RPAS estimations were within 0.10 m for 8 of the 12 SD validation measurements. Negative SD values in output SD DEMs were attributed to vegetation compression in bare earth DEMs. Increasing the spatial resolution of DEMs from 0.05 m up to 10.24 m impacted SD estimations as follows: most detail was lost at 10.24 m resolution, while at 1.00 m only minor changes centred mostly on maximum SD estimations occurred and the minimum and mean remained almost unchanged. At the coarsest resolution of 10.24 m, both the

maximum and minimum RPAS SD estimations converged close to the mean, which remained almost unchanged.

Bühler et al. (2016) compared SD distributions in two small plots within a Swiss ski area. A single snow surface survey was conducted at a 0.25 km^2 ridge top plot, while three were conducted in a 0.12 km^2 alpine valley. Ground cover consisted of mostly rocky outcrops and grass, with sparsely distributed trees and small bushes present in the valley plot. A custom octocopter RPAS equipped with a camera modified to capture images at a constant altitudes of 97 – 157 m above the ground, with image overlap set to 70% was used. Primarily natural landmarks were used as GCPs, augmented by 10 targets that were set out by field crew. Manually measured SD ranged from near zero to over 4.5 m. At the valley bottom site, a negative bias of 0.20 m was reported, with a RMSE of 0.25 m. In areas were there was minimal vegetation, the RMSE was just 0.07 m, however, the RMSE increased to 0.30 m in areas containing tall grass and shrubs. At the ridgetop site, a negative bias of 0.11 m was found, and a RMSE of 0.15 m. The authors note that vegetation caused the bare earth DEM to have overestimations of elevation, leading to underestimations of SD.

In Western Canada, Harder et al. (2016) reported highly accurate SD estimates in a multi-temporal study of alpine and prairie landscapes. The alpine survey site consisted of 0.32 km^2 of sparsely vegetated rocky terrain with slope angles ranging from ~ 15° – 35°. As with other alpine study sites noted above, wind transport caused SD to be highly variable, with snow-free areas neighboured by snow drifts as deep as 5 m. Excluding snow-free areas, the mean SD was 2 m. The prairie site consisted of 0.65 km^2 of agricultural land covered in wheat stubble of varying heights. A shallow, homogenous, snow cover of around 0.2 – 0.3 m with a maximum manual

measured depth of 0.5 m was present, as well as bare patches. At both sites, a fixed wing RPAS equipped with RTK GPS were flown ~ 90 m above the ground, collecting images with an overlap of 70 – 85%. Tarps measuring 2.3 X 1.3 m in size and natural objects were used as GCPs. At the prairie site, 22 flights were conducted throughout the melt period in March 2015, while bare earth flights were conducted during several days in early April. At the alpine site, 18 flights were conducted during the melt period between May 15th and June 24th, as well as four flight of the bare earth surface on July 24th. Validated against manual SD measurements, the overall accuracy of SD at each site was reported as RMSE, with 0.085 m found at the alpine site, and 0.137 m at the prairie site. While the manufacturer of the RTK GNSS equipped RPAS that was used indicated the inclusion of GCPs was unnecessary, including GCPs during post-processing improved the mean absolute error from 0.27 m to 0.10 m at the prairie site, and from 0.14 m to 0.06 m at the alpine site; however, the standard deviation of error was minimally affected. Over-exposed imagery that occurred due to the significant presence of snow-free ground at the alpine survey location in the winter, and during spring snow melt at the prairie site, was addressed by removing overexposed pixels to reduce point cloud errors.

Bühler et al. (2017) tested the utility of using a RPAS equipped with a Sony NEX 7 system camera to estimate SD in challenging snow and light conditions during individual snow surface surveys at two separate study areas in the Swiss and Austrian Alps. To expand the Near Infrared Reflectance (NIR) range of the camera, the standard NIR filter within the APS-C CMOS sensor was removed, which allowed a range of λ 350-1100 nanometers. Both survey sites were 0.12 km^2 in size and located in mostly flat alpine valleys, with some short trees and shrubs present. Data from the Austrian site was also used in Bühler et al. (2016). Both a fixed wing and

rotor RPAS equipped with modified cameras able to capture RGB and NIR imagery were used. Flight elevations ranged from 100 – 150 m above the ground, and SD varied from bare ground on plowed roads to ~ 1.5 m in depth. Additionally, at the Austrian site, a terrestrial laser scanner was used for validating RPAS SD estimates. Notably, the SD DEM with the lowest RMSE at 0.17 m came from the RGB dataset, compared to RMSE of 0.20 m and 0.23 m for DEM derived from NIR imagery. The authors surmise this was due to the NIR data generating a greater amount of points during SfM processing, which can present more outliers that in turn increase RMSE. Further, spray-on GCPs were not visible in the NIR830 band, forcing the use of DEMs that GCPs were visible within to line then up, possibly introducing error from mismatching of coordinates. The NIR dataset excelled in areas where the snow surface was homogenous or illumination was poor, producing unfiltered point clouds with far less noise than the RGB dataset.

Cimoli et al. (2017) provide a concise and detailed account of their multi-site study in Svalbard and Western Greenland during the spring and summer of 2015, where they tested the utility of using a consumer grade RPAS to map SD. Six small low elevation plots consisting of bare soil and boulders with minimal vegetation and ranging in size from 0.0014 km^2 to 0.1457 km^2 were examined. A diversity of snow conditions and depths of up to 3 m were measured. During snow surveys, the RPAS was flown at very low elevations, ranging from 7 – 26 m, with snow-off flights ranging from elevations as low as just 2 m, all the way to 1500 m; image overlap was set to ~ 80% at the front, and 60% to the side. A combination of placed and natural GCPs were used, varying in numbers from 3 – 11 per survey. RMSE of estimated SD ranged from 0.059 – 0.18 m, and were generally negatively biased. The use of images in large RAW

format instead of JPEG for DEM creation was also tested in this study, with RAW format increasing the number of matched points within the point cloud by only 6 – 7%, but at a cost of greatly increased processing times.

Conducting a multi-temporal SD survey over two winters in northwestern Italy, Avanzi et al. (2018) compared RPAS SfM and multi-station laser scanning techniques. The 0.0067 km^2 study area was located in a grassy alpine area with scattered rocks, two watercourses, and a building. A rotor RPAS was used to conduct flights 60 m above the ground, with images captured at 70 – 90 % overlap. GCPs used were referenced to a permanent GNSS station to achieve accuracy as high as 0.06 m after post-processing. To validate RPAS and multi-station estimates, 135 and 115 manual snow measurements were collected during the two individual field season respectively; with SD to ~ 1.5 m, RPAS estimates during the first winter resulted in RMSEs of 0.17 m – 0.45 m, while in the second winter, the RMSE was reduced to 0.06 m when creek beds and areas of tall grass that contained high error values were excluded as outliers from the analysis.

Utilizing a RTK GNSS equipped fixed-wing RPAS, Revuelto et al. (2021) conducted seven field campaigns, during which they tested SD retrieval accuracy under different lighting conditions and flight parameters without the use of GCPs. A terrestrial laser scanner was used as the primary method of validating RPAS-SfM SD estimates. The 0.48 km^2 study area was located in the Spanish Pyrenees, and consisted of irregular grass covered terrain, which including gullies and ridges at elevations between 2000 – 2300 m. SD varied from zero to over 4.5 m in drifts. When light conditions were ideal (full, mid-day sun), a RMSE of 0.19 m was found, which was similar to that of other studies utilizing GCPs, while under poor lighting conditions the RMSE

increased to as high as 0.77 m. Additionally, the testing of multiple flight parameters showed that lighting conditions were the key factor controlling accuracy. A change of only a few centimeters RMSE occurred when flight elevation was increased from 120 m to 200 m, and photo overlaps were reduced from 85 % sidelap and 90 % frontlap, down to 70 % sidelap and 85% frontlap. These time saving adjustments to flight parameters, i.e. elevation increase and overall decrease in GSD, are recommended by Revuelto et al. (2021), going against recommendations from several other studies.

Working to improve RPAS SfM accuracy within forests, Harder et al., (2020) compared RPAS LiDAR and RPAS - SfM methods in two sparsely forested plots located in Western Canada, one located in the Prairies and, and the other in the Rockies. A LiDAR unit was flown on a DJI M600 Pro rotor RPAS 100 m above the surface on parallel flight lines with 80 m of separation, collecting 75 points per m^2. Flights for SfM processing were done using a fix-wing RPAS flown at 120 m above the surface with image overlap set at 80% frontlap and 65 % sidelap. LiDAR based SD estimates were consistently negatively biased, while SfM based SD estimates were both positively and negatively biased. As with other studies (Lendzioch et al., 2016), it was found that RPAS SfM methods are incapable of reliably estimating SD within closed canopy forested areas, with RMSE ranging from 0.20 – 0.33 m in such areas. Results from the RPAS mounted LiDAR were found to consistently produce a RMSE of less than 0.17 m within forested areas. LiDAR results from open areas of this study produced RMSE ranging from 0.09 m – 0.10 m, while SfM outputs resulted in RMSE of 0.10 m – 0.30 m across the same plot. While SfM results in open areas were in the range of previous literature, the authors

definitively state “that UAV (RPAS) SfM is fundamentally inappropriate to sense sub-canopy surfaces (Harder et al., 2020).”

2.3 Other RPAS Survey Applications

Examples of applications of SfM-derived DEMs from RPAS in other landscape applications are included here for breadth and context. Of particular interest to SD RPAS practitioners is the work of glaciologists who use RPAS in difficult flying conditions, dangerous terrain access, and low contrast lighting that can result in low point matching levels in outputs (Bhardwaj et al., 2016; Gindraux et al., 2017). Growth in the use of RPAS by glaciologists has been somewhat slow due to the inherently challenging atmospheric conditions faced during alpine and high latitude research (Bhardwaj et al., 2016). In the Peruvian Andes at elevations of over 4000 m, Wigmore and Mark (2017) used a custom made RPAS to tackle the challenging low pressure flying conditions of their high elevation study area, showing that it is possible to conduct SfM surveys at very high elevations. In their multi-temporal study, sub-centimetre accuracy was achieved while documenting flow velocity, elevation changes, and change in mass of the glacier examined. Specifically, GCP error was under 0.025 m, while DEM errors were just 0.002 m and 0.003 m in the first and second year of the study respectively. Across their study plot, they calculated 156,000 m^3 of ice loss, and mean elevation change of -0.75 m; maximum loss was 18.0 m near the calving face, while increases of 11.5 m were seen elsewhere. The terminus location remain unchanged between the two years. Ely et al. (2017) conducted high resolution RPAS SfM surveys over recently deglaciated landscapes in northern Sweden, producing high accuracy locational results with DEM RMSE of ~ 0.05 m. The high accuracy

results allowed detailed geomorphological maps of the newly ice-free terrain to be produced for use as a baseline to monitor how the new landscape changes over time.

Outside of cryosphere and SD mapping, DEMs created through SfM processing of RPAS captured images have been used to conduct landscape monitoring around the world. E.g. Lucieer et al. (2014) studied a slow moving, multi-month landslide in Tasmania, producing results with overall DEM RMSE of 0.04 m and 0.08 m during two separate survey dates. High precision DEMs to 0.01 m were produced, allowing detailed height changes within the slide area to be detected, as well as the mapping of flow direction and displacement magnitude to be conducted. While monitoring a multi-year landslide in Southern Spain, Fernández et al. (2016) used novel methods in combining RPAS captured imagery and standard GIS displacement measurement techniques, with semi-automated processes to measure the horizontal movements of olive tree centroids being displaced in the slide area. With a mean horizontal displacement of up to 2.8 m per year, the overall XY mean error of the digital surface model was ~ 0.02 m, while Z was ~ 0.06 m, with RMSE of 0.10 m for XY and 0.13 m for Z was found in an analysis of the complete five year dataset. Error was limited to near centimetric values in some portions of the study. Many other examples of terrain differencing using RPAS exist, and can offer insight for RPAS SD mapping, particularly during the snow-off surveys.

2.4 Sources of Error

2.4.1 Impacts of Low-Laying Vegetation on SD Accuracy

Perhaps the biggest challenge to overcome in using RPAS-SfM to estimate SD is the potential for significant error introduced by the presence of continuous low lying shrubby perennial vegetation. New growth and plants that rebound as the snowpack melts can result in

negative values being generated when bare earth DEMs are subtracted from snow-surface DEMs (Jagt et al., 2015; Lendzioch et al., 2016; Nolan et al., 2015). A basic explanation follows. Where perennial vegetation is sparse, it is possible to remove isolated shrubs from bare earth DEMs, however, when it is thick and continuous, SfM processing results in DEMs where the top of the shrub layer is misidentified as the bare earth. This results in an elevated bare earth that is then compressed by the snow, resulting in an underestimation of depth ie a negative bias. Quantifying this bias remains a key challenge.

In trying to address accuracy problems associated with vegetation being misidentified as the ground, Jagt et al. (2015) rejected manual SD measurements believed to be erroneous due to underlying shrubs, and applied a multi-scale curvature classification filtering technique, which removed sparsely distributed trees from the point cloud, however, the shared characteristics between low lying vegetation and the terrain in their study area prevented shrubs and grass from being detected and removed. Lendzioch et al. (2016) replaced negative values caused by vegetation rebound that appeared in their initial results with lowest manually recorded snow measurements; they also report that single trees caused distortion within the snow surface DEMs, resulting in snow estimate discrepancies. To minimize errors related to vegetation regrowth and rebound, snow free surveys for bare earth DEMs should be conducted as close as possible to the ablation of the snowpack (Bühler et al., 2016).

While expensive, LiDAR data can be effective in creating higher accuracy snow free DEMs that can reduce the level of error introduced by vegetation (Cimoli et al., 2017; Deems et al., 2013; Harder et al., 2020; Jagt et al., 2015; Wainwright et al., 2017). In areas where perennial

vegetation growth is insignificant, an individual LiDAR dataset could prove to be effective in producing snow-free DEMs for multi-year RPAS SD studies (Jagt et al., 2015).

2.4.2 Point Matching & NIR Sensors in RPAS SfM SD Surveys

Mapping of snow covered terrain using SfM processes can be challenging due to the low contrast nature of the snow surface in imagery, causing poor featuring-matching (Cimoli et al., 2017; Gindraux et al., 2017; Tonkin & Midgley, 2016). This issue is most pronounced with images containing freshly fallen snow, shadowed areas, and during flat light conditions (Cimoli et al., 2017; Gindraux et al., 2017; Tonkin & Midgley, 2016).

Gindraux et al. (2017) found remarkably different levels of point matching when comparing freshly fallen snow to day old snow in the same plot with consistent lighting conditions. For fresh snow, when 20 images were used in SfM processing, only 2 of 20 images were oriented during the image orientation step in the SfM workflow, resulting in just 143 point matches being detected in the initial alignment, and 115,250 point matches detected in the dense point cloud. Waiting a day for the fresh snow to settle enhanced contrast and produced much better results, with 19 of 20 images being oriented, 15,400 point matches detected in the initial alignment, and 1,032,700 point matches detected in the dense point cloud. This analysis exhibits clearly that if fresh snow has fallen, RPAS-SfM SD survey flights should be delayed for at least one day. Further analyses should be conducted to test the impact of snow aging on SfM processing results.

By using NIR sensors in bands 700 nm and 830 nm, as well as a pan-chromatic 350-1100 nm band, Bühler et al. (2017) were able to largely overcome challenges related to snow reflectance variability. While most insolation in the visible portion of the electromagnetic

spectrum is reflected, the majority of NIR energy is absorbed by snow, allowing NIR sensors to capture fine details by detecting differences in snow grain size. This, and less saturation in NIR images helps to create higher accuracy DEMs, particularly when illumination is poor, and recent snowfall has occurred. Drawbacks that may exist in conducting surveys with only NIR energy would be orthophotos that are more difficult to interpret over those of produced using RGB imagery, possible challenges in matching coordinates to GCP within NIR imagery, and high costs compared to RGB based RPAS methods.

2.4.3 GCP Considerations

Highly precise georeferencing is essential to producing accurately georeferenced point clouds from SfM outputs, and is especially important when conducting change detection analysis (Wainwright et al., 2017). The most common method to achieve this is by using centimetre accuracy RTK GNSS devices to record GCP locations consisting of targets set out throughout the survey area, and/or landmarks visible in images captured during RPAS surveys (Jagt et al., 2015; Nolan et al., 2015; Wainwright et al., 2017). GCP targets most commonly used in snow research are checkered or ‘X-shape’ patterns painted on wood or printed on plastic (Harder et al., 2016; Wainwright et al., 2017). The use of natural or human built objects can augment or replace temporarily placed targets, but the potential of winter snow obscuring them should be carefully considered (Avanzi et al., 2018). To save the time it takes to collect GCPs distributed across a survey area after RPAS flights, Bühler et al. (2017) used spray paint to mark GCPs directly on the snow surface; while this technique worked for RGB images, it was noted that the blue spray paint they used did not appear in the 830 nm NIR band imagery as the paint absorbed an equal amount of radiation as the adjacent snow surface (Bühler et al., 2017). This is the only example

found of spray paint being used to make GCPs in SD RPAS surveying, however, it is commonly used to make GCPs in non-snow RPAS surveys. Given that SD surveys are often carried out in sensitive mountain watersheds, non-toxic dissolvable GCP options are desirable.

To date, the quantity of GCPs varies significantly between studies, with a minimum of 10 generally being deployed (Bühler et al., 2017; Cimoli et al., 2017; De Michele et al., 2016; Harder et al., 2016; Lendzioch et al., 2016). While investigating optimal GCP placement and quantity, Tonkin and Midgley (2016) found vertical RMSE increased to 0.156 m when three or less GCPs were used, but when increased to four, a vertical RMSE improved to 0.064 m. Interestingly, vertical RMSE actually increased to 0.076 m when 15 GCPs were used, and with 101 included, only decreased to 0.059 m. Uniformity of GCP placements was noted to impact RMSE, with errors increasing to over 0.10 m when GCPs were placed more than 100 m apart from each other. While conducting an accuracy assessment of DEMs produced using RPAS data of glaciated and snow covered terrain, Gindraux et al. (2017) found similar results to Tonkin and Midgley (2016), noting that accuracy within DEMs decreases by about 0.09 m per 100 m of distance from GCPs. Gindraux et al. (2017) found that when GCPs were clustered and/or placed far apart, the impacts of radial camera lens distortion and resultant doming (dome shaped deformations) in output DEMs is reduced, further highlighting the need to distribute GCPs evenly. In addition to using RGB imagery, Miziński and Niedzielski (2017) measured SD using NIR sensors without the use of GCPs, producing a mean absolute error of 0.33 – 0.43 m, and a RMSE range of 0.41 – 0.58 m for SD estimates; it should be noted that the mean validated snow depth in Miziński & Niedzielski, was 0.41 m, with a range of 0.24 – 1.06 m (2017). So far,

omitting GCPs for RPAS SD surveys introduces unacceptable error levels, and should be left for projects that require less accurate results.

2.4.4 SD validation

Validation of RPAS derived SD estimates by manual measurements is the standard practice to quantify errors in SfM processing and change detection analysis (Adams et al., 2017; Avanzi et al., 2018; Jagt et al., 2015; Lendzioch et al., 2016; Nolan et al., 2015). Different approaches for manually measuring SD include random spot checks, transects, and measurements at GCPs (Adams et al., 2017; Lendzioch et al., 2016; Nolan et al., 2015). In a highly detailed study that utilized crewed aircraft over three large study areas of 50 km^2, Nolan et al. (2015) manually collected ~ 6000 depth measurements using a GNSS-enabled probe, called *Magnaprobe*, which stores coordinates with ~ 5 m precision and SD to ~ 0.02 m precision.

Common challenges noted while conducting manual SD measurements include vegetation below the snow creating uncertainty as to the real ground location and representative SD, and the presence of buried ice layers that can be mistaken for the ground (Avanzi et al., 2018; Jagt et al., 2015). Avalanche danger and challenging terrain can prevent the collection of SD validation measurements in sections of some study areas (Girod & Filhol, 2020). Collecting an RTK GNSS coordinate at both ends of a transect with a measuring tape between them to precisely space SD measurements is a potential time saving method that could be utilized not noted in RPAS-SfM SD literature. Another method not noted in RPAS-SfM SD mapping studies is the use of snow stakes to collect SD validation data, however, it is a well established method used to measure snow at individual locations (Bongio et al., 2021; Collados-Lara et al., 2019; Collados-Lara et al., 2017) .

As LiDAR can produce DEMs with high accuracy, it can be used for both validating RPAS-SfM SD measurements, and for use as a bare earth DEM in static landscapes where a single dataset can be utilized for multiple years (Cimoli et al., 2017; Deems et al., 2013). As noted above, in addition to SD validation, LiDAR datasets are particularly useful when addressing vegetation-related errors, particularly under forest canopy; however, LiDAR pulses can fail to penetrate through thick ground covering shrubs, leading to similar error levels seen in RPAS-SfM results (Deems et al., 2013; Harder et al., 2020). Because the resolution of LiDAR datasets are typically much lower than those produced by RPAS-SfM, nessesary interpolation processes between points can introduce error when subtracting a snow-off LiDAR DEM from a higher resolution snow surface RPAS-SfM DEM (Deems et al., 2013). As with RPAS-SfM derived DEMs, SD estimates from LiDAR derived DEMs also show greater error levels when vegetation is present (Harder et al., 2020).

While comparing SD estimates from RPAS mounted LiDAR with RPAS-SfM SD estimates, Harder et al. (2020) found that sub-canopy RPAS LiDAR results were significantly more accurate, noting that SfM methods are not appropriate for measuring sub-canopy SD. While the cost of RPAS LiDAR equipement is far greater, they state that the added cost is nessesary to measure SD under the forest canopy, as RPAS-SfM can only be used in open areas, meaning sub-canopy estimates must be interpolated from SD estimates in surrouding open terrian. In open terrian, differences in accuracy between LiDAR and RPAS-SfM SD estimates are minimal, therefor, where trees are absent, RPAS-SfM may be desirable over RPAS LiDAR given the greatly reduced cost and relative simplicity of use.

2.4.5 SWE Measurement

Few examples exist where RPAS derived SD has been used to estimate SWE across a study area (Niedzielski et al., 2019). In open, but sheltered lower elevation coastal areas, snow density can be much less variable than SD because the usually high moisture level of snow in such areas hinders the transport of snow by wind that can result in higher variability of density and formation of dense slabs (Avanzi et al., 2018; McClung & Schaerer, 2006). Because of this, in protected and low elevation coastal regions, it may be practical to extend RPAS-SfM derived SD estimates to SWE by using the mean SWE density from point measurements (Avanzi et al., 2018; Sturm et al., 2010).

A novel approach tested by Yildiz et al., (2021) combined RPAS-SfM survey methods with Ground Penetrating Radar (GPR) derived density to estimate SWE across a low angle 1 ha study plot in the Ilgaz Mountains, located in Turkey. Ground cover consisted of grass, shrubs, and scattered fir and pine trees. Off-the-shelf rotor based RPASs were used to conduct surveys for SfM processing. Bare earth and snow surface surveys were flown at 80 m and 150 m, with GSD of 2.5 cm and 3.5 cm respectively. GPR transects were done by towing the unit behind a snowmobile, as well as by hand, with results being used to determine the mean snow density. Standard snow-tubes were used to collect manual SWE and SD measurements for validation. SWE maps were created by multiplying the SD raster and calculated mean snow density of 355 kg/m^3, producing a RMSE of 0.063 m from the 80 m flight, and 0.069 m from the 150 m flight relative to manual SWE measurements, which had a mean of 366 mm.

2.4.6 RPAS Types

Of the 12 RPAS-SfM SD survey studies discussed above, fixed wing RPAS were used exclusively in four, while multi-rotor RPAS were used exclusively in six; as discussed above, Revuelto et al., (2021) compared a commercial grade fixed-wing and two off-the-shelf multi-rotor RPAS, with error levels of output from each platform found to be virtually the same. Harder et al., (2020) utilized a large multi-rotor RPAS to fly the heavier LiDAR payload and a fixed-wing for an RGB camera. Both primary types of RPAS have pros and cons. The main advantages of fixed wing RPAS are greater flight times of up to 45 minutes, and fast flight speeds of up to 100 km/h (Harder et al., 2016; Whitehead et al., 2014) . A major disadvantage of most fixed wing RPAS is the requirement of a fairly large take-off and landing area (Whitehead et al., 2014). Further, because most fixed-wing RPAS are simply landed on their belly with no landing gear, they require a generally dry, flat, smooth surface to land on, meaning powder or wet snow surfaces could be problematic (Revuelo et al., 2021). Fixed wing RPAS are not capable of making the very tight turns that rotor RPAS can make, which is an important consideration when flying SfM surveys. Additionally, most fixed-wing RPAS are not capable of handling the larger payloads of different sensors such as LiDAR (Harder et al., 2020).
The bulky size of some fixed wing RPAS can make them difficult to transport when study plots are located in remote foot or ski access only locations; some may even be too large to fit into a helicopter.

Rotor RPAS have greater maneuverability, allowing tighter grids to be flown, have much better obstacle avoidance capabilities, can hover, and perform better in windy conditions. Because rotor RPAS take off and land vertically, they require a much smaller area for

deployment and landing (Revuelto et al., 2021), Further, the speed control of rotor RPAS is far superior to that of fixed wing types. The main disadvantage of rotor RPAS is their lower flight time of ~ 20 – 30 minutes, which requires landing them multiple times to switch batteries during surveys of large study areas, thus increasing field time and reducing the amount of data that can be collected at midday when lighting is ideal.

2.4.7 Flight Parameters

To achieve a comparable GSD, lower resolution cameras need to be flown closer to the ground than high resolution ones. In the reviewed SD studies, GSD ranged from 0.01 cm to 5.3 cm. Because of the low contrast nature of snow, a high GSD is essential for ensuring an adequate level of point matching when doing SfM processing. Because lowering flight elevation also increases flight time to cover an equivalent area significantly, finding the optimal GSD is an important part of planning RPAS snow surveys. GSD is automatically calculated and displayed in flight planning software such as *Map Pilot Pro* (Drones Made Easy, 2021).

Typically, RPAS surveys are flown at a constant height, which is based on the elevation of the take off point. This approach works when surveying generally flat terrain, but in hilly or mountainous areas, this can cause large variations in GSD, as well as increase the risk of RPAS damage from crashing into steep slopes or cliffs. Flight software such as *Map Pilot Pro* contain an option called *terrain aware*, whereby reference DEMs are used as reference to keep the RPAS elevation nearly constant relative to the ground. Because most reference DEMs have a nominal resolution of 25 m, caution must be exercised in areas containing cliffs because it is possible small terrain features may be missed in this relatively course resolution. Practitioners can also create their own DEMs, making terrain aware flights much more precise. To date, the use of

terrain aware flight planning software is not noted in the literature covering RPAS SfM SD mapping.

Flight patterns of most SfM surveys consist of an overlapping double grid pattern (Bhardwaj et al., 2016; Hugenholtz et al., 2013). As noted above, gimbled cameras on RPAS are generally set to forward facing downward angles of 70 - 90 degrees from the RPAS body, with image overlaps of 80 – 85 % to ensure good coverage (Gaffey & Bhardwaj, 2020). James and Robson (2014), recommend the use of off-nadir angle imagery to reduce doming distortion that can be common in imagery from consumer-grade RPAS cameras. Fraser and Congalton (2018) note that flying below 50 m can result in a quick loss of connection to the remote controller, and loss of line-of-sight which is required by law in most jurisdictions. They also found that flying at 50 m above the ground resulted in greatly reduced image alignment success and average matching per image when compared to more common flight elevations of around 70 - 100 m.

2.5 Summary

The preceding chapter provided a review of the relevant literature to identify key knowledge gaps and inform specific research questions. In this fast growing discipline, new research is being published regularly on the subject of RPAS-SfM SD mapping; at the time of this writing, all known relevant peer-reviewed RPAS-SfM SD mapping articles are discussed, while others that examine relevant subjects including, RPAS, SfM, LiDAR, and cryosphere research in general are touched on.

Most of the existing literature in this field primarily describes RPAS-SfM surveys in generally simple terrian, which contains limited, or no vegetation (e.g. De Michele et al., 2016; Bühler et al., 2017; Cimoli et al., (2017). As shown above, accuracy levels vary greatly. In

vegetated areas, greater error is reported due to vegetation that is compressed under the winter snowpack being misidentified as ground in bare earth models where it rebounds, creating negative bias. Where snow is deeper, relative error is reduced. Due to the additive nature of error in SfM-DEM terrian differencing, 0.10 m accuracy of SD estimates is considered good. Where surveys have been done with thick vegetation present, high error values that are sometimes greater than the manually measured SD have been observed (Jagt et al., 2015; Lendzioch et al., 2016), while Harder et al. (2020) highlight that RPAS-SfM SD survey methods are not capable of producing useful outputs under forest canopy. No literature exist where RPAS-SfM SD mapping has been applied in recently logged or burned terrain, or on the Pacific coast of North America in general.

When using RPAS technology to estimate SD, many factors must be considered including hardware types, GCP network design, validation methods, and flight parameters. Rotor RPAS are favoured in many studies due to their flexible flight abilities and compact size, while fix-winged RPAS and their greater battery life are used in easy to access areas with flat terrian available for landing (Revuelto et al., 2021). The even distribution of GCPs is an important when conducting RPAS-SfM surveying (Gindraux et al., 2017; Tonkin & Midgley, 2016). If GCPs are clumped together, or less than 4 GCPs are used, high DEM error can occur; even distribution so that no areas within SfM surveys are more than 100 m from a GCP can be expected to produce DEM outputs with RMSE of 0.10 m or under (Gindraux et al, 2017). In locations where some surfaces stay snow-free during the winter, natural objects have been used as static GCPs, however, no examples exist of permanent above-snow GCPs being installed. Weather and snow surface conditions are important to consider when planning field campaigns. When new snow

has recently fallen, the level of point matches in SfM outputs is greatly reduced, which in turn increases DEM error and uncertainty of SD estimates (Gindraux et al., 2017). Deep shadowing and low sun angle are also known to increase error levels (Cimoli et al., 2017; Gindraux et al., 2017; Tonkin & Midgley, 2016).

While application of SWE to RPAS-SfM SD estimates is so far limited within the literature (Niedzielski et al., 2019), it is a fundamental measurement used in water management, and should therefore be further explored (Avanzi et al, 2018).With improvements to approaches being developed frequently, the standard workflow continues to shift as different areas with different ground cover and terrain types are examined.

Chapter 3: Study Area and Methods

3.0 Study Area Description

This study took place in the Russell Creek Experimental Watershed (RCEW), situated at 50°19' N, 126°21' W on northeastern Vancouver Island within the Tsitika River Watershed (Figure 1).Vancouver Island is large mountainous island located on the west coast of Canada, which is characterized by a maritime terrestrial climate with moderate temperatures, high annual precipitation totals, and frequent winter snowfall at higher elevations where snowpack depths of over 3 m are common (CHRL, n.d.; Snow Survey Data - Province of British Columbia, n.d.).

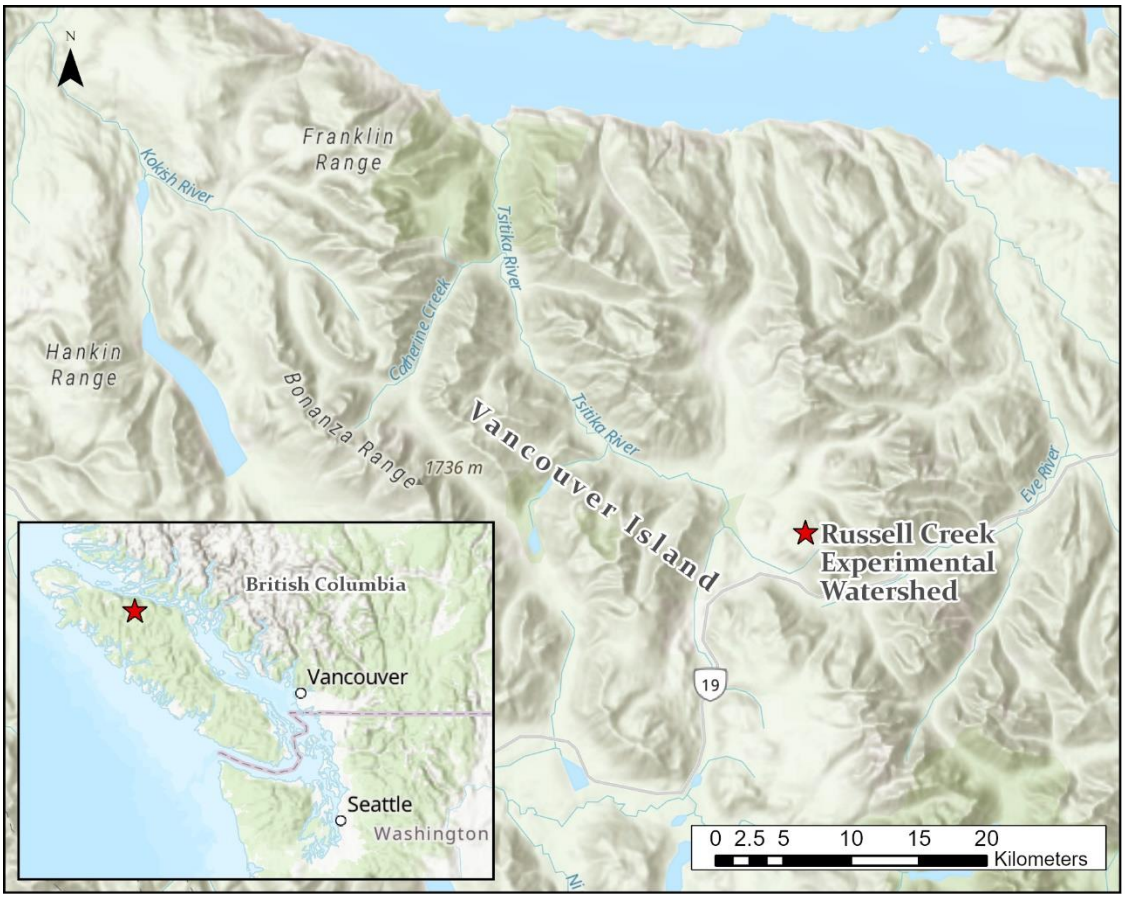

Figure 1. Study area location on northeastern Vancouver Island

The Mountain Hemlock (MH) biogeoclimatic zone covers the upper elevation of the RCEW. On Vancouver Island and the adjacent mainland coast, forest is continuous to the upper ranges of the MH, which exists from 900 - 1800 m asl within the region. Seasonal snow is generally above 600m asl, with episodic snow down to sea level during some years. The MH dominant tree species are Mountain Hemlock (*Tsuga mertensiana*), Yellow Cedar (*Cupressus nootkatensis)* and Amabalis Fir (*Abies amabilis)*. Higher elevations of the MH zone transition to parkland where large forest openings are interspersed with low subalpine vegetation such as pink mountain-heather (*Phyllodoce empetriformis*) and blue-leaved huckleberry (*Vaccinium deliciosum)* (Meidinger & Pojar, 1991). Annual precipitation in the MH ranges from 1700 to 5000 mm, with 20 – 70% percent falling as snow, resulting in deep snowpack regularly lasting into the summer. At 1650 - 1800 m asl, the MH zone transitions to the Alpine Tundra (AT) zone (Meidinger & Pojar, 1991). The AT zone is found on only the highest peaks of Vancouver Island and the immediate mainland coastal mountains, and is devoid of trees except at the lower edge where groups of stunted trees referred to as krummholz are located. These forest ecosystems extend down the Pacific coast from SE Alaska in the north, to Oregon in the south.

RPAS field campaigns were conducted in May and June of 2020, and March, April and May of 2021. The plot within the RCEW chosen for this study is 0.56 km^2 in area, with an elevation range of 900 – 1300 m, and an average slope angle of 25° (Figure 2). The dominant aspect is westerly, with much of the higher elevation eastern section being WNW, while southwestern portions consist primarily of northerly aspects (Figure 2). Much of the study plot was logged in 2008, and then replanted in 2010 with Yellow Cedar and Mountain Hemlock. There are four old growth stands of trees within the cutblock, consisting of Mountain Hemlock,

Amabalis Fir and Yellow Cedar. The plot margins are surrounded by the old growth forest in all directions except along the northern margins, where regenerating stands are present from an adjacent cutblock.

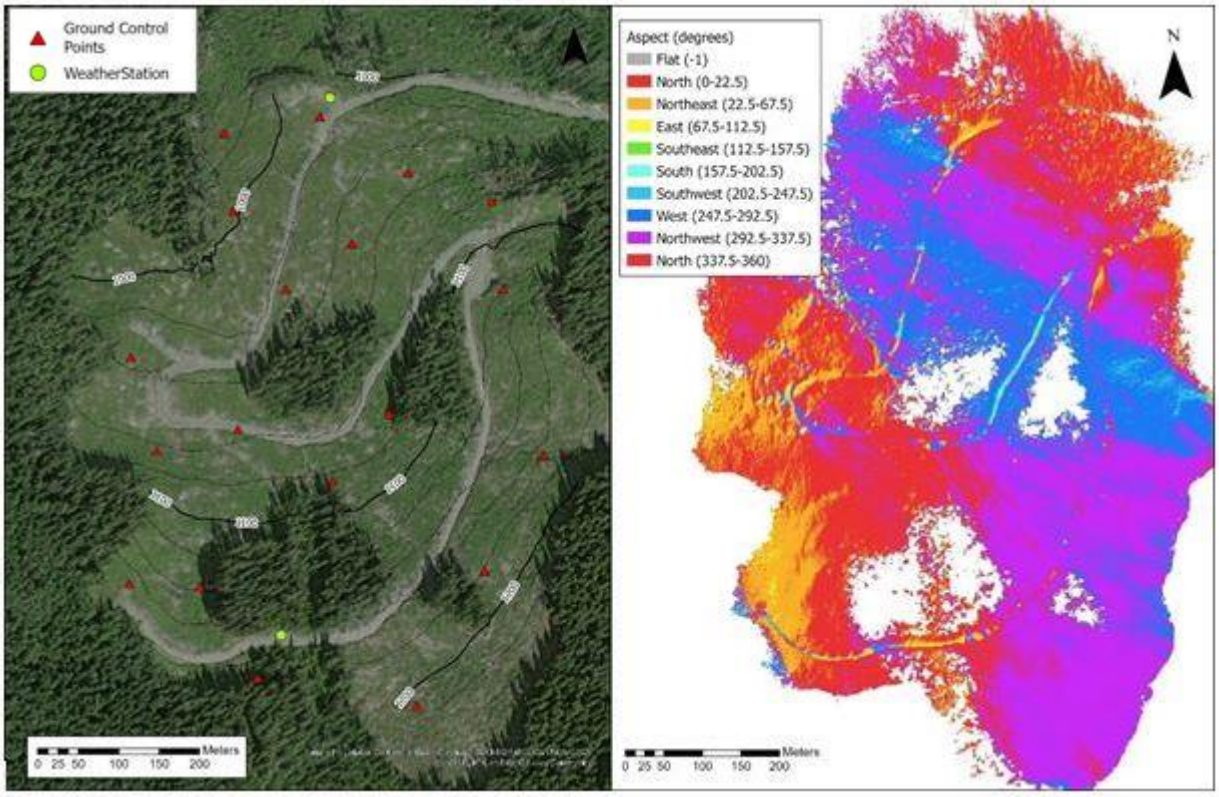

Figure 2. Orthophoto of the study plot in April, 2021 with contours (generated from output DEM of this study) and ground control points (left). Study plot aspects (right)

Replanted trees are still relatively small, at heights to ~ 2 m, while old growth trees within, and surrounding the study plot reach heights of ~ 30 - 40 m. Throughout harvested sections, a large number of stumps, as well as slash piles and fallen logs are found (Figures 3). In addition to being useful for GCP installation, the presence of static, above-snow, objects, such as stumps and logging debris was identified in previous studies as being useful for verifying DEM alignment and accuracy (Cimoli et al., 2017; Jagt et al., 2015). A stream running through the centre of the

plot, which remains largely open throughout the winter, also aids in DEM alignment and accuracy assessment.

Figure 3. Aerial views of summer and winter conditions at the Russell Creek Experimental Watershed Study Plot

3.1 Study Area Climate

The RCEW is a long-term research installation managed by the British Columbia Provincial Government Research Program. Research in the RCEW is primarily focused on the impacts of forest management and climate change on watershed hydrology. Hydrometeorological data has been recorded here since 1995 across a network of eight remote automated weather stations across an elevation range of 493 – 1516 m; two of these weather stations are located within the RPAS study plot. In the upper portion of the RCEW where this study took place, the snowpack typically becomes established in November or December, and peaks in March or April, with snow melt commencing shortly after and lasting into the early summer. Mean annual precipitation at 1100 m in the RCEW is ~ 2300 mm, the vast majority of which occurs during the fall, winter, and spring months (Wang et al., 2016). Winters in the RCEW are moderate, with above freezing temperature and rain-on-snow events occurring regularly. Typically, a few short lived Arctic outbreaks invade the area each winter, bringing

temperatures that can drop below -10°C, however, in winter (Dec, Jan, Feb) the mean temperature is -1.1°C (Wang et al., 2016).

3.2 Field Seasons Weather & Snowpack Conditions

After a warmer than average December, weather conditions were only slightly above normal in the region throughout the 2019/2020 winter. Spring 2020 began with below average temperatures in March, before shifting to above average in April and May (Pacific Climate Impacts Consortium, 2021). Overall, precipitation levels throughout the winter months were close to normal, however, the arrival of moisture laden storms was concentrated in January with precipitation levels of over ~ 100 % of normal being measured. Spring 2020 was drier than normal, particularly in April when almost no precipitation arrived at all until the last week of the month (Pacific Climate Impacts Consortium, 2021).

As with the early winter of the first field season, December began with slightly above normal temperatures, which continued into January (Pacific Climate Impacts Consortium, 2021). February was markedly colder, with the monthly average ~ 3°C below normal, and below average precipitation. The cooler than normal weather continued into March, before temperatures shifted to above average in mid-April. Precipitation levels throughout much of the spring were well below the seasonal averages across the southern half of the province.

3.3 Methods

3.3.1 Summary of methods

Field methods are given in Section 3.4 and lab-based methods are given in Section 3.5. A general overview of the project workflow is show in Figure 4.

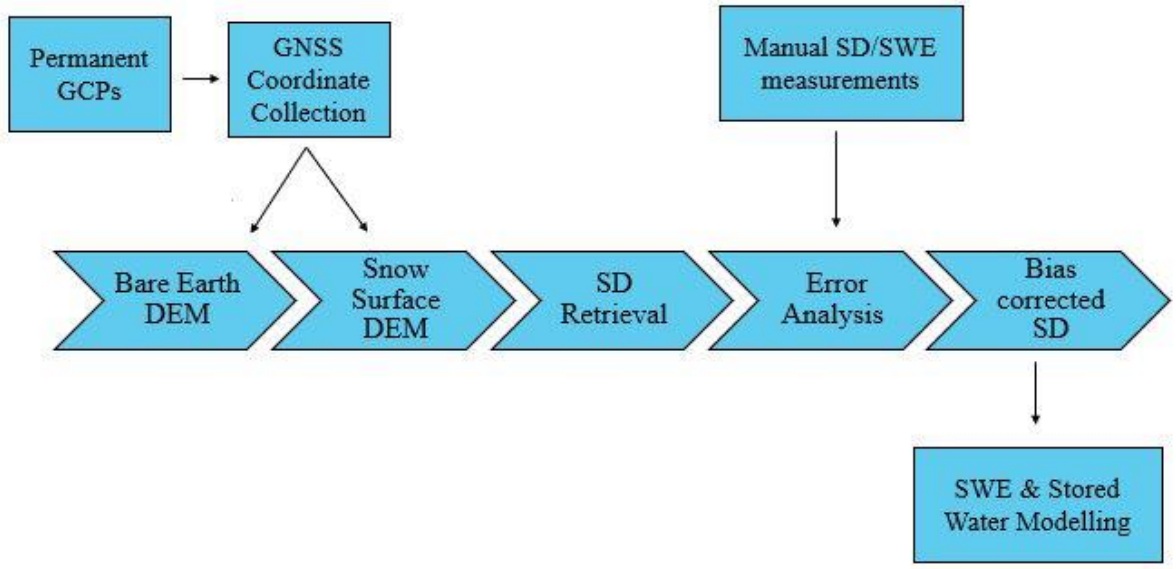

Figure 4. Workflow summary. Global Navigation Satellite Systems (GNSS) coordinates are collected at Permanent Ground Control Points (GCPs). GCP coordinates are inputted during Structure from Motion processing and into Digital Elevation Models (DEM). Snow depth (SD) is calculated by subtracting the Bare Earth DEM from the Snow Surface DEM. Manual SD and Snow Water Equivalent (SWE) are used for assessing error of DEM derived estimates. A bias correct is then applied before SWE and stored water modelling in completed.

3.4 Field Methods

3.4.1 GCP Installation

In November 2019, 18 custom made aluminum GCPs were installed prior to the arrival of the seasonal snow-pack. These GCPs consist of a flat cross pattern welded on top of a 140 cm tube (Figure 5). The cross pattern was painted bright orange, with a matte finish to prevent glare from obscuring RPAS photos. The initial paint coating quickly chipped off most GCPs due to improper surface preparation. Prior to repainting in fall 2020, surfaces were sanded before applying a spray-on, self-etching primer, then matte orange alkyd enamel spray paint. With this preparation, the painted surface remained intact throughout the next winter. In the centre of the cross pattern, threads were welded in place to affix GNSS units to, which aids in the collection of

high precision and accuracy base and rover coordinates. GCPs were installed by fastening attached base plates to four hanger bolts drilled into existing stumps (Figure 5). This design allowed for the GCPs to be level after installation by adjusting the nuts on the hanger bolts.

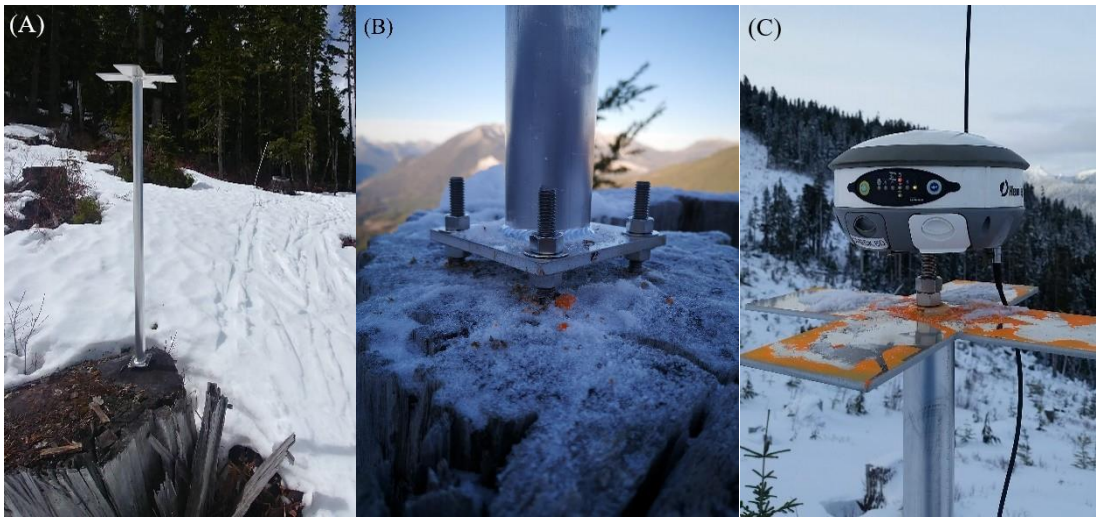

Figure 5. Installed GCPs at RCEW. (A) Full GCP. (B) Mounting bracket at the base secured to stump using hanger bolts, with nuts and washers used to level the target. (C) GNSS head secured to threaded GCP centre using a threaded rod. Note the chipped paint surface during the winter of the first field season.

Permanent GCPs were positioned approximately 200 m apart to minimize distortions and ensure the best accuracy possible (Gindraux et al., 2017; Tonkin & Midgley, 2016). The layout of the installation was created by covering a DEM of the study area with 100 m radius circles, then designating centre points as installation locations (Figure 2). In the field, GCPs were installed as close as possible to these points to ensure good distribution while picking prominent, rot-free stumps. Since little information on above-snow surface permanent GCP placement exists, additional temporary snow surface GCPs (fabric and stencil) were deployed during initial surveys. Stencil targets were created using readily available, non-toxic, and inexpensive powder (paprika) that did not require retrieval upon completion of the RPAS flights, thus reducing survey times considerably. While it was found to work well within several hours of application,

warm temperatures did cause some distortion in the targets through melting, increasing uncertainty in GCP coordinate matching during SfM processing. To reduce this uncertainty during above-freezing temperatures, RPAS flights were conducted immediately after application of the targets.

3.4.2 GCP RTK GNSS Collection

Coordinates were collected using two *Hemisphere s320* survey grade RTK GNSS units, one as a base station, and the other as a rover unit. A single GNSS base location was established utilizing a permanent GCP as a static platform to collect sub-centimetre precision and accuracy coordinates during three 24 - 48 hour collection periods. A GNSS rover unit linked to the base station was used to collect coordinates across the GCP network. The rover unit was threaded onto permanent GCPs and left to collect coordinates for a minimum of 120 seconds. At temporary GCPs, a monopod was used with coordinate collections of a minimum of 30 seconds. Throughout the RTK coordinate collection process, it was ensured that the connection between the rover and base station maintained a "fixed" solution status, with a Position Dilution of Precision (PDOP) of less than 4. A low PDOP value, indicates that satellites are well spaced across the sky, which is essential for capturing high accuracy coordinates (Natural Resources Canada, 2013). Higher PDOP values result in lower accuracy positional results.

3.4.3 Flight Equipment and Parameters

A DJI Phantom 4 Pro V2 was the primary RPAS flown during this project, with a DJI Phantom 4 Pro being used during surveys in the 2020 field campaign (DJI, 2021). The flight software package *Map Pilot Pro 4.1.2*, installed on a *Ipad Mini 4* connected to the aircraft controller, was used to plan and launch flight missions (Maps Made Easy, 2021). A *terrain*

aware function in the flight control software (described above) was used to fly the RPAS at a relatively constant height to maintain the target GSD of 2.5 cm and 2.8 cm across the complex terrain of the RCEW study area. The base DEM used for the *flight aware* terrain function is derived from the Shuttle Radar Topography Mission, which has an output pixel size of 30 m. Therefore, caution must be exercised when using *terrain aware* around steep topographic features, as well as trees and buildings.

3.4.4 RPAS Data Collection

Data collection consisted of four snow surface campaigns, and two bare earth field campaigns, which are here-after identified as SNOWYY-MMM for (snow surface surveys), GROUND2020 for (bare earth surveys) (Table 1). Due to the COVID-19 pandemic, planned winter and early spring field campaigns were cancelled for the 2020 field seasons. After several months of delay, institutional permissions were granted to resume, and fieldwork was able to commence. Due to the delay, surveys of peak snow coverage and winter snow conditions were not possible during the 2020 field campaign, however, the resumptions of fieldwork in early May allowed one snow surface survey to be conducted while most of the study plot was still snow covered.

Field trips were scheduled when cloud-free and low-wind weather conditions were forecasted. When possible, snow surface RPAS surveys were conducted several days after snowfall events to allow the snowpack to settle and become more favorable for SfM. To reduce anticipated vegetation induced errors, bare earth RPAS surveys were conducted as close to full snow ablation as possible, i.e., before vegetation had completely rebounded or significant new growth had occurred.

3.4.5 SD and SWE Measurements

Graduated avalanche probes (1cm increments) were used to collect SD measurements, while SWE measurements were collected using standard 3.87 cm diameter federal snow samplers. Measurement locations were distributed across the study area to account for different aspects, slope angles, and forest canopy effects. Sample plots were largely based on a scaled down version of the 'X' shaped plot structure used by Jost et al. (2007), where two transects were done in cardinal directions from a shared centre point. In Jost et al. (2007), transects were 60 m in length, with SD recorded at 1 m intervals, and SWE recorded at 3 m intervals, however, based on findings from a 2019 pilot field trip (Appendix 1), SD and SWE sample points were reduced, while transect lengths and layouts were changed to improve efficiency. SD and SWE measurement transect layouts included 1) Cardinal plots with 10 m transects and 2.5 m sample spacing coming from a shared centre point (Figure 6a) , 2) using GCPs as a centre point with 3 SD and 1 SWE measurements conducted lined up with the cross pattern 3.0 m from the centre of GPCs (Figure 6b), and 3) L shaped plots with a shared centre point and two 12 m transects with 1.0 m sample spacing (Figure 6c) During the second field season, transects across roads and into adjacent off-road areas were conducted to enable quantification of variations in accuracy across different ground cover types, while the use of the L shaped plots were no longer used in favor of the cardinal plots, which were also being utilized in a concurrent LiDAR research project in the RCEW. When time permitted, supplementary linear SD transects at random locations were conducted on an opportunistic basis throughout the study plot.

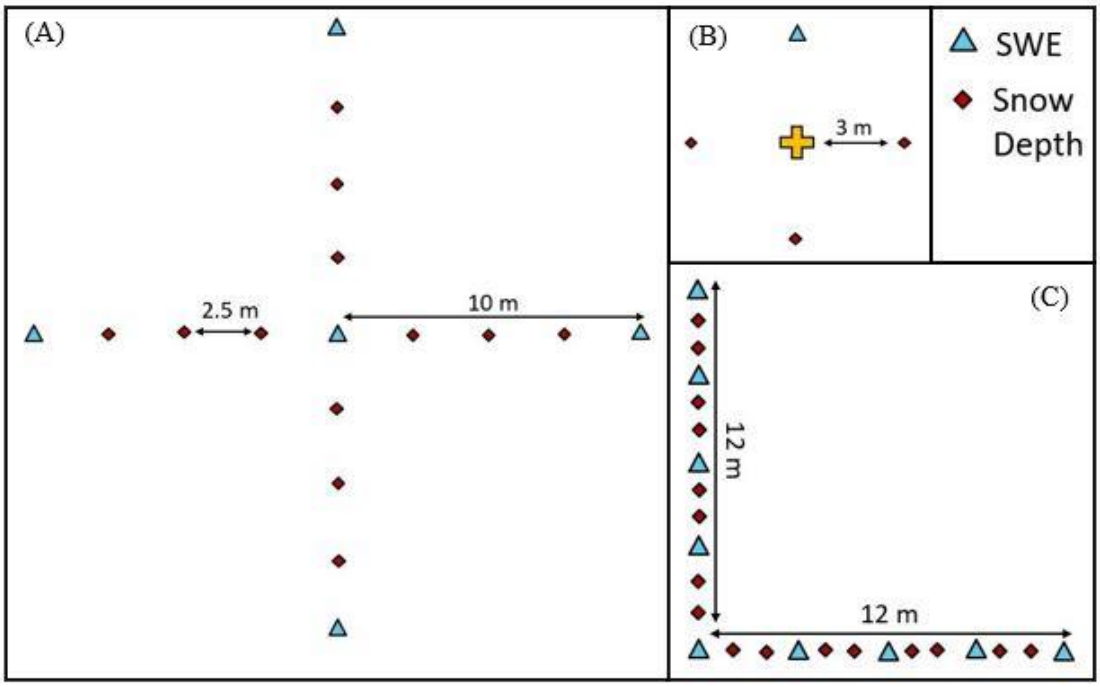

Figure 6. Snow depth and SWE sample plot designs. Cardinal plot (A), four point plot centred on permanent ground control points (B), and L-plot with one transect positioned uphill-downhill and the other across slope (C).

SD and SWE sample points were marked with paprika to make them visible in RPAS images for matching during post processing. Doing so removed the need to conduct time consuming RTK GNSS coordinate collections at snow measurement plots. This, combined with having permanent GCPs established, meant that RTK GNSS equipment could be left behind if desired to save crew labour time. However, the concurrent research project taking place in the RCEW meant RTK GNSS equipment was always brought on-site, and therefore available for spot checks. These spot checks showed sub-centimeter horizontal differences between collected coordinates and visually matched measurement locations during post-processing.

3.5.0 SfM Processing: Alignment and Sparse Cloud Generation

The SfM processing included five primary steps: 1) initial photo alignment 2) sparse cloud generation 3) dense point cloud generation, 4) DEM generation, and 5) orthophotograph generation (Figure 7). Agisoft PhotoScan Pro 1.5.2 was chosen for SfM processing under guidance of Fraser et al., (2018) who noted it produces results with greater accuracy than Pix 4D, the primary alternative SfM software package used in this field. First, blurred images were removed prior to SfM processing. The coordinate system assigned to images by the RPAS were converted from latitude and longitude to UTM NAD 83 to match the collected RTK GCP coordinates. Images were aligned using the "high accuracy" setting in Agisoft, which gives the best possible initial camera position estimates in the sparse cloud, and highest possible number of point matches during this step (Agisoft, 2022). Upon completion of the alignment and sparse cloud processes, GCP marker coordinates were imported, typically appearing within 1 m of their location in the image. Next, GCP marker coordinates were manually centered on their associated GCPs visible within images.

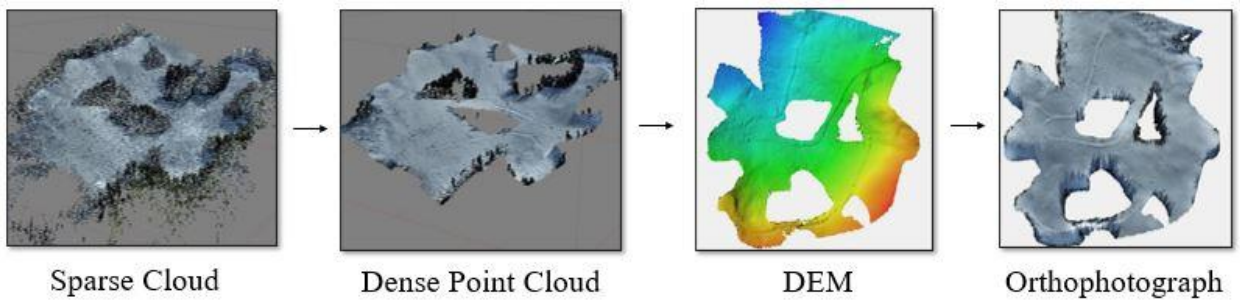

Figure 7. The four primary Structure from Motion and Digital Elevation Model processing steps conducted within Structure from Motion processing software.

3.5.1 Dense Point Cloud Generation

Before proceeding to dense point cloud generation, margins of the study plot and forested areas within it were masked and excluded from further analysis as they were found to be heavily distorted, and introduced vertical and horizontal distortion in adjacent open areas during preliminary SfM processing. Within forest stands in and around the study plot, the ground was mostly not visible through the very dense canopy; deriving snow depths from slight openings produced unreliable and extremely erroneous SD values varying from -5 m to 20 m. After this, a combination of manual and automated processes were used to remove noise and misaligned points within the sparse point cloud. Low precision coordinates assigned to each image during RPAS flights and used for the initial alignment were not included in the final positioning during dense point cloud generation, leaving only the high precision and accuracy RTK GCP coordinates to be used. To reduce computation time, the dense cloud generation parameter was run at the low quality setting, meaning pixel size would be reduced from that of the GSD, producing DEMs with a final pixel size of 19 cm. The pixel size of orthophotographs remained the same as the GSD of 2.5 – 2.8 cm.

3.5.2 Snow Depth and Snow Water Equivalent Calculation and Validation

The bare earth DEM was subtracted from and snow surface DEMs to produce gridded SD models. Next, validation points were matched to their locations using collected coordinates, or by visual matching. Pixel values of SD were subtracted from SD validation points to calculate error (detailed below). To account for the impact of vegetation rebound, field validation data was used to calculate bias, which was then used to vertically adjust the DEMs where vegetation was present. Within the bare earth orthophotograph, vegetated areas were identified using an object

based supervised classification process conducted in *ArcGIS Pro 2.9*. The default schema from the *national land cover dataset* was utilized (ESRI, 2022). Three rounds of training were conducted using the *segment picker*. Vegetation was combined into two classes (trees and shrub) while a third class was identified as road, which captured road sections, and other vegetation free areas. A stratified random accuracy assessment of the classification results was conducted to determine the quality of the classification process. SWE estimates were derived from corrected snow surface DEMs by multiplying the mean snow density from manual SWE measurements by the SD DEM to produce SWE DEMs covering the study plot, which were then used to calculate total water stored as snow.

3.5.3 Error Analysis

Error can occur in numerous steps throughout the RPAS-SfM SD surveying workflow. In the field, GNSS accuracy and precision can be affected by terrain features or trees blocking satellite paths. Discrepancies in SD measurements can occur if field crews mistake ice layers for the ground, or drive the probe beyond the snowpack and into the ground. While SD validation measurement errors are difficult to quantify, experienced and well trained field crew minimized this type error from being introduced during field campaigns. To check for error in manual SD measurements, and to check for melt on warms days when some time had passed between measurements and RPAS flights, spot check re-measurements were conducted by re-measuring SD at the exact locations of earlier measurements.

Reports generated within *Agisoft* give vertical, horizontal, and total error values for generated DEMs, calculated GCP location error, reprojection error, pixels error, and camera (RPAS position) error. Differences between manual SD measurements and RPAS SD estimates,

as well as manual SWE measurements and RPAS derived SWE estimates, were used to determine error of RPAS-SfM SD estimates. This error analysis is divided into vegetated and non-vegetated areas; validation points were divided into road and off-road areas, and by bare earth and vegetated ground cover, while all plot types were grouped together. Error is presented as RMSE, bias, mean absolute error (MAE), and mean relative error (MRE). Bias, as calculated below in equation (1) is the mean of all absolute error values, and communicates if there is bias within SD estimations, and if so, what direction such biases are.

$$\text{bias}(\hat{y}) = sd_{y}\ (\hat{y}) - y \quad (1)$$

Where $\hat{y}$ represents DEM snow depth or snow water equivalent estimates, and y represents manual measurements. If a consistent bias is identified, than this is used to systematically adjust snow surface DEMs using a vertical offset. Following this, RMSE shown in equation (2) is calculated, which generally represents random error. RMSE communicates the spread of SD estimate error, both between individual surveys, and different ground cover areas within them. Additionally, RMSE is also used to communicate DEM error as determined by differences between GCP coordinates and their projected positions within point clouds.

$$RMSE = \sqrt{\sum_{i=1}^{n} \frac{(\hat{y}-y)^2}{n}} \quad (2)$$

Where **n** represents the number of points being compared, in Digital Elevation Model error assessment**,** $\hat{\mathbf{y}} - \mathbf{y}$ represents the difference between point cloud projections and high accuracy coordinate points collected during field campaigns. MAE, shown in equation (3) is calculated by

changing all absolute error values to positive, before calculating the mean, showing the absolute error value across the dataset, and within different areas of outputs.

$$MAE = \frac{1}{n} \sum_{i=1}^{n} | y - \hat{y} | \quad (3)$$

Equation (4) shows MRE, which gives the error relative to the manually measured SD, and communicates how error becomes greater when SD is lower.

$$MRE = \frac{1}{n} \sum_{i=1}^{n} \left| \frac{y - \hat{y}}{y - \hat{y}} \right| \quad (4)$$

Chapter 4: Results & Discussion

4.1.0 Environmental Conditions: Field Seasons

Both field seasons shared similar weather characteristics, which included extensive periods of mostly above freezing air temperatures with regular rain-on-snow events interrupted by Arctic outbreaks in January and February (Figures 8 & 9). March 2020 began cool before a significant warm-up occurred, while during March 2021 a cool active weather pattern persisted, with regular snow events throughout (Figure 9). The abrupt arrival of warm sunny periods occurred in April of both field seasons. The snowpack gradually gained height throughout both winters, before peaking at 1.99 m on March 10th in 2020, and 2.31 m on April 10th in 2021 at the upper weather station. SWE recorded 10 km to the south at an automated weather station located at 1260 m a.s.l peaked on March 4th in 2020, and April 10th in 2021 (Figures 8 & 9). The warm, sunny periods during mid-April of both field seasons triggered rapid snow melt, with full ablation occurring by early May at the lower weather station (1017 m a.s.l) during both seasons, and by late May in 2020, and early June in 2021 at the upper weather station (1171 m a.s.l). Strong winds occurred regularly throughout both field seasons. During the 2019-2020 field season, mean winds at the exposed lower weather station were 6.01 m/s, and 0.73 m/s at the more sheltered upper station; in the 2020-2021 field season, mean wind speed was 5.13 m/s and 0.79 m/s at the lower and upper weather stations respectively.

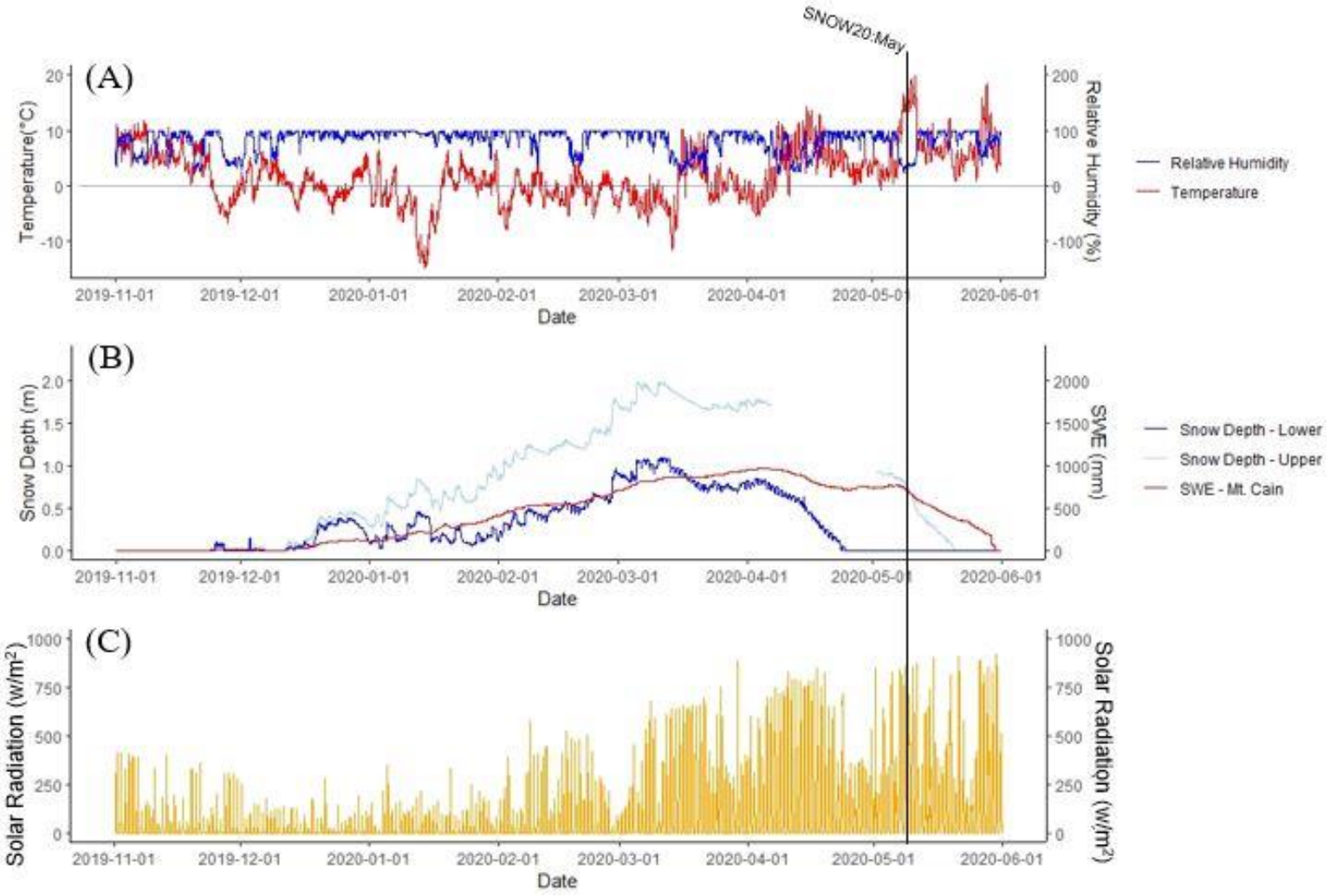

Figure 8. Weather and snow conditions throughout the 2019-2020 snow season at weather stations in the study plot at 1017 m (lower) and 1127 m (upper), as well as at 1130 m from nearby Mt. Cain. 2 m air temperature and humidity was recorded at the lower weather station (A), with snow depth and SWE recorded all three (B), and incoming solar radiation at the lower station (C)

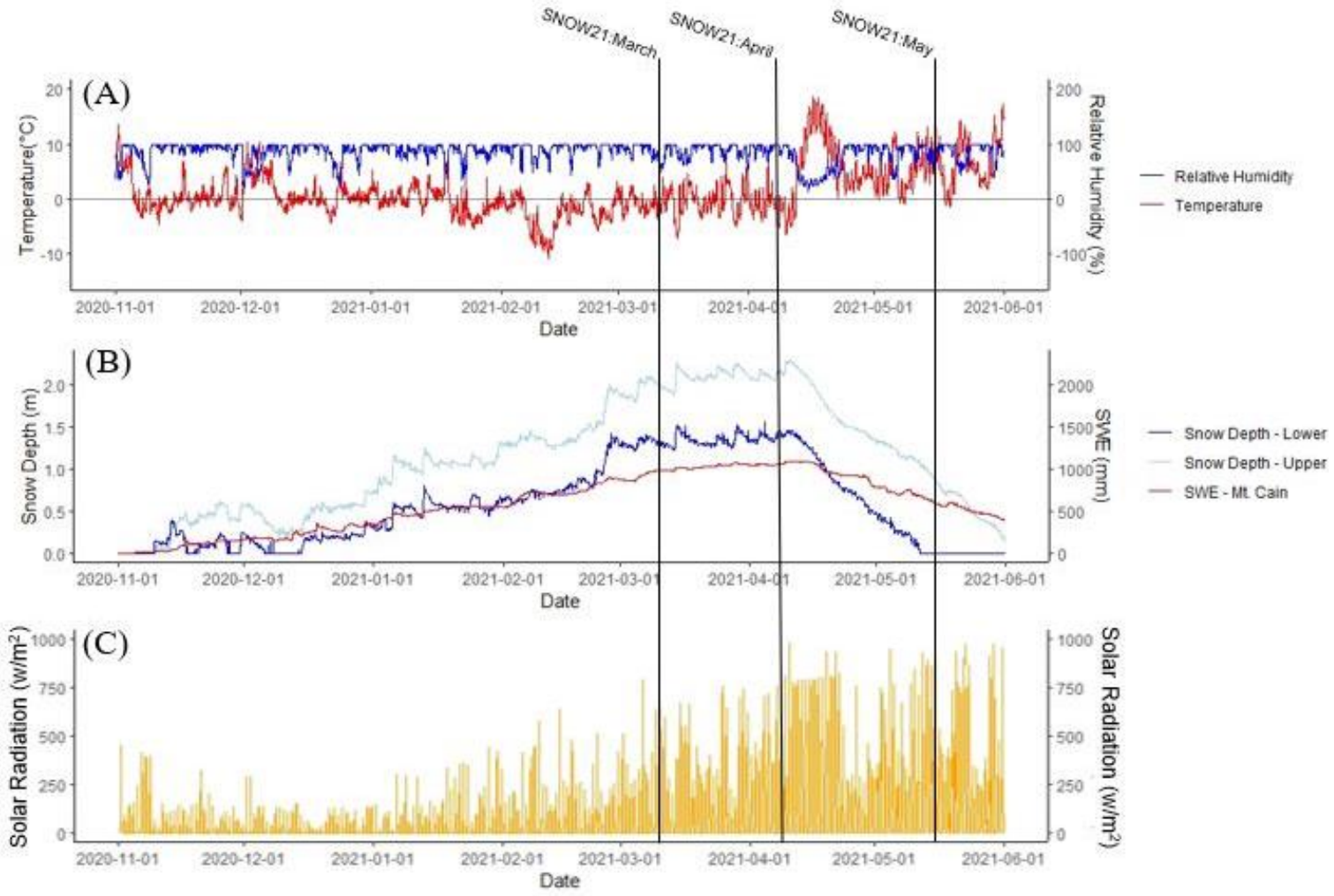

Figure 9. Weather and snow conditions throughout the 2020-2021 snow season at weather stations in the study plot at 1017 m (lower) and 1127 m (upper), as well as at 1130 m from nearby Mt. Cain. 2 m air temperature and humidity was recorded at the lower weather station (A), with snow depth and SWE recorded all three (B), and incoming solar radiation at the lower station (C)

4.1.2 Environmental Conditions: Field Campaigns

Varied snow conditions were encountered throughout the four snow surface field campaigns; isothermal and melt-freeze conditions persisted during SNOW20:May and SNOW21:May, while during SNOW21:March and SNOW21:April, the snowpack was cold with the surface consisting of primarily undisturbed recently fallen snow (Table 1). Arriving at the study plot for the first snow surface survey, (SNOW20:May) the ground was found mostly snow

covered, with stumps and slash piles protruding above the snowpack, and several sections of road exposed in the lower half of the study plot. With no new snow in the previous weeks, and being later in the spring, the snow surface had developed a deep suncup texture and was littered with lichens, needles, twigs, and branches that had fallen from the surrounding forest. Very similar snow surface conditions were encountered during SNOW21:May, but with greater SD and snow covered area . During both the SNOW21:March and SNOW21:April field campaigns, full snow coverage was found, with only parts of large fallen trees, very tall stumps, and slash piles protruding through the snow surface. By design, winds were generally light throughout all field campaigns days, and with the exception of SNOW21:March, lighting conditions were bright and consistent (Table 1).

Table 1. Environmental conditions during RPAS surveys recorded at the lower weather station at 1017 m a.s.l near the bottom of the study plot.

Survey ID	Light Conditions	Solar Radiation (W/m^2)	Solar Elevation	Temperature Range (°C)	Wind Range (m/s)	Snow Surface Conditions
SNOW20:May	Sunny	795	55.19°	Low: + 0.5 High + 16.5	3.5 – 11.9	Freeze-thaw; forest litter
SNOW21:March	Sun and cloud	628	32.81°	Low: - 3.7 High: + 3.8	4.2 – 11.2	Fresh snow
SNOW21:April	Sunny	716	43.50°	Low: - 2.1 High: + 0.5	3.5 – 7.5	Fresh snow
SNOW21:May	Sunny	862	55.34°	Low: + 6.5 High: + 13.4	1.4 – 5.6	Freeze-thaw; forest litter
GROUND2020	Sunny	858	57.86°	Low: + 5.9 High + 18.4	2.1 – 11.9	Freeze-thaw; forest litter

4.2.0 Validation Measurements and RPAS Flights

A total of 511 SD measurements and 170 SWE measurements were collected throughout the four individual snow season field visits. During SNOW20:May, 22 spot checks of samples ~ 24 hours after initial measurements showed zero to minimal changes of 0.01 – 0.05 m between measurements, which was likely due to snow melt. Similarly, random spot checks during SNOW21:May showed changes of 0.07 m or less. Of the 170 SWE measurements used here, 50 were collected at weather stations located within the plot as part of an ongoing long term climate and hydrology monitoring program at RCEW.

Double grid flights were conducted capturing oblique images at 10 – 20° off-nadir angles to reduce the potential of doming distortions occurring, with 70% side lap and 90% front lap along track (James & Robson, 2014). Flights were performed on relatively calm sunny days, as close to solar noon as feasible, when shadows were least prevalent, and lighting was consistent across the study plot (Table 1). Under these flight parameters, GSD ranged from 2.29 – 2.49 cm per pixel when flown at 70 m, and 2.69 – 2.80 cm per pixel when flown at 80 m (Table 2). Owing to the large size of the study plot, surveys were broken up into multiple 5 – 8 hectare sections, which required one to two RPAS batteries per section**.** Because complete snow melt occurred several weeks earlier at lower elevations and in steep sections, bare earth imagery from field visits on May 27th – 29th, and June 16th and 17th was utilized to create bare-earth point clouds and DEMs (GROUND2020) with the least amount of new vegetation growth as possible.

Table 2. RPAS survey dates and ID, number of GCPs included in post-processing, assigned flight altitude, resultant GSD, and area surveyed.

Date	Survey ID	GCPs	Flight Altitude (m)	GSD (cm)	Coverage Area (km2)
6-8 May 2020	SNOW20:May	15	70	2.29	0.44
9 March 2021	SNOW21:March	16	70	2.69	0.33
5 April 2021	SNOW21:April	12	80	2.74	0.36
14-15 May 2021	SNOW21:May	15	80	2.49	0.53
27-29 May 2020	GROUND2020	18	70	2.43	0.28
16-17 June 2020	GROUND2020	18	70	2.43	0.28

4.3.0 DEM Results

Thick, ground-covering, perennial vegetation that covers 73 % of the surface (as determined by an orthophoto classification) was misclassified as the bare earth surface throughout much of the study plot, creating a snow-free DEM that is subsequently compressed by the winter snowpack. Figure 10 shows the smooth surface of the dense point cloud that the bare earth DEM was derived from. SfM processing was unable to discern vegetation from the ground, creating this smooth surface. The top of the vegetation layer being classified as the surface throughout much of the study plot caused a systematic negative bias of SD estimates, however, this bias is minimal, non-existent, or shows slight positive bias where vegetation is absent on road surfaces, and bare patches within off-road areas. Differences in elevation between both SNOW20:May and SNOW21:May DEMs and the GROUND:2020 DEM at 296 identical samples points extracted from small sections of bare-earth visible in both snow surveys show minimal disagreement; relative to the GROUND:2020 DEM, in SNOW20:May, a negative bias of -0.073 m exists, while in SNOW21:May, a slight negative bias of -0.006 m is seen. These minimal discrepancies can be attributed to noise within individual DEMs within vegetation free

bare earth areas. To better understand vegetation height and the potential for bias, two vegetation transects with 68 individual vegetation height measurements spaced ~ 3 m apart were conducted in the centre of the study area, running SW-NE and S-N. When excluding the bare sections from these transects, a mean vegetation height of 1.09 m with a standard deviation of 0.43 m and median of 0.99 m was observed. The maximum shrub height was 1.34 m, while trees up to a maximum height of 2.80 m were recorded. 19 of the 68 measurements consisted of bare earth.

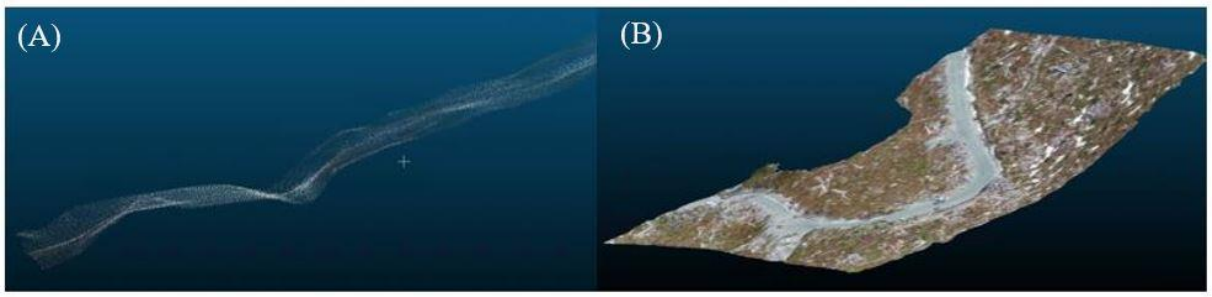

Figure 10. (A) Close up of the bare earth dense point cloud showing a relatively smooth surface created by thick vegetation, which is not differentiated from the ground. Note the flat portion left of centre which is road surface. (B) Zoomed out view of the same area of the dense point cloud.

DEM accuracy calculated from SfM processing ranged between 0.013 m RMSE for the bare earth DEM, and up to 0.221 m RMSE in SNOW20:May (Table 3). SNOW21:May, which occurred under similar conditions as SNOW20:May but with slightly more snow cover, returned a RMSE of 0.083 m and vertical error of 0.028 m. The RMSE of SNOW21:March and SNOW21:April were similar at 0.179 m and 0.191 m respectively, however, large portions of SNOW21:March contained deep shadowing, which caused excessive noise (misplaced pixels) in point clouds, and areas of extreme error of over 2 m in RPAS SD estimates. The lower number of images captured during SNOW21:April due to images only being captured on half of the transects during two flights in the centre of the study plot resulted in less point matches overall, and high reprojection error, which is the RMSE of differences in distance between key points

(distinct features within an image) and tie points (distinct features identified and matched in multiple images) in images (Agisoft, 2022). When contrast is low, such as was found in SNOW21:April, greater discrepancies between tie points and key points is more likely, which appears as noise within point clouds (Table 3). However, despite this, DEM results were still acceptable with a overall RMSE of 0.191 m . Relative to the number of images used, the point match totals during SfM processing were much greater during snow-on surveys when no recent snowfall had occurred, and during snow-off surveys.

Table 3. Structure from Motion output results.

Survey ID	Camera Stations	Points Matches	Projections	DEM RMSE (m)	Estimated GCP Vertical Error (m)	Reprojection Error (pixel)
SNOW20:May	3244	3,768,985	12,112,764	0.189	0.045	1.19
SNOW21:March	2314	1,152,925	3,277,678	0.179	0.120	2.86
SNOW21:April	1598	979,854	2,960,938	0.191	0.065	10.9
SNOW21:May	2587	1,618,312	8,079,506	0.083	0.028	1.40
GRD20:May	3156	2,250,599	7,600,757	0.013	0.005	1.18
GRD20:June	3156	2,250,599	7,600,757	0.013	0.005	1.18

When comparing DEMs and orthophotos, varying degrees of horizontal misalignment between different dates were visible. In most datasets, misalignments ranged from sub-centimetre to 0.10 m; greater misalignments of up to 1 m were concentrated near DEM edges, and on the NE edge of the study plot where the terrian is particularly steep and complex, with forest stands nearby. Such misalignments are likely due to doming distortion within point clouds that are often present at edges of RPAS survey areas (James & Robson, 2014; Gindraux et al., 2017). To reduce the impact of doming effects, images were collected beyond the edge of the

study plot so that problematic areas could be masked out without removing areas of interest within DEMs.

4.4.0 RPAS SD Estimates Overview

SD outputs consisting of DEMs with 19 - 22 cm pixels show extensive spatial variation of SD across the study plot, from bare earth to over 4 m. Accuracy of results vary widely within individual surveys. Best agreement between RPAS-SfM SD estimates and individual SD validation measurements of generally 0.10 m or less are found on road sections, while in thickly vegetated areas, differences varied from less than 0.10 m to as great as 0.74 m (Table 4; Figure 11). Error metrics for each survey are broken up by area in Table 4 below. Within all datasets, there exists a negative bias in off-road areas resulting in RPAS-SfM derived SD being consistently underestimated. On road sections in SNOW21:April and SNOW21:May, a negative bias of - 0.10 m and -0.09 m exist, while in SNOW21:March, there is a positive bias of 0.10 m. In off-road sections, a negative bias of - 0.25 m was found in SNOW20:May, -0.31 m in both SNOW21:March and SNOW21:May, and - 0.46 m in SNOW21:April.

Table 4. RPAS SD estimate error values. Note that SNOW20:May contains no on-road validation points.

Dataset	Terrain Type	Number of SD Validation points	Bias (m)	MAE (m)	MRE (%)	RMSE (m)
SNOW20:May	All	173	- 0.25	0.32	29	0.38
SNOW20:May	Road	0	n/a	n/a	n/a	n/a
SNOW20:May	Off Road	173	- 0.25	0.32	29	0.38
SNOW20:March	All	53	- 0.21	0.37	17	0.44
SNOW21:March	Road	12	0.10	0.27	18	0.30
SNOW21:March	Off Road	41	- 0.31	0.39	17	0.45
SNOW21:April	All	107	- 0.28	0.33	14	0.42
SNOW21:April	Road	47	- 0.10	0.14	7	0.15
SNOW21:April	Off Road	60	- 0.46	0.50	19	0.59
SNOW21:May	All	145	- 0.15	0.17	18	0.21
SNOW21:May	Road	86	- 0.09	0.07	9	0.08
SNOW21:May	Off Road	59	- 0.31	0.32	26	0.36

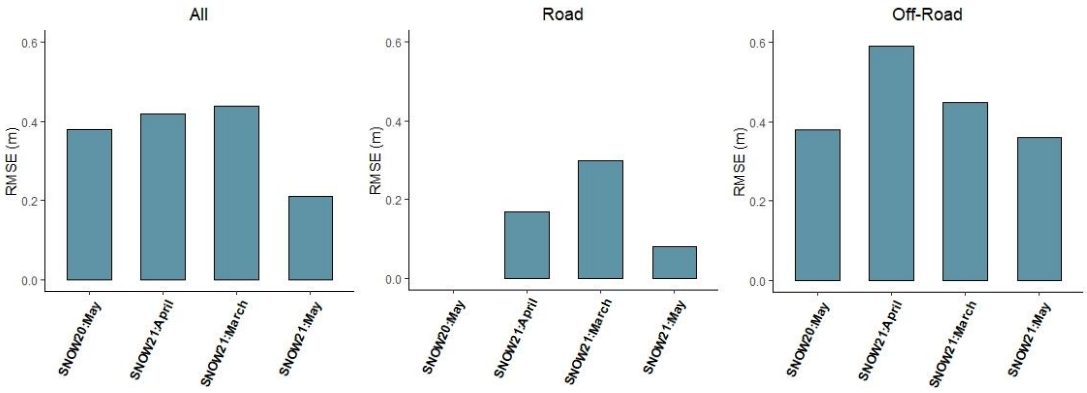

Figure 11. RMSE of difference between RPAS estimate and validation snow depth in all datasets, and terrain types. Note that SNOW20:May does not have road transect validation points.

Thick vegetation throughout the RCEW study plot, distortions near DEM edges, and shadowing in SNOW21:March caused numerous outliers to exist within the initial comparisons of RPAS-SfM SD and manual SD measurements. Outliers that fell above or below two standard deviations from the error mean of each survey dataset were removed, which resulted in 29 out of 511 validation points being omitted from error analysis. Most outliers were confined to off-road areas

and the NE corner of the study plot. The presence of deep shadowing shown in Figure 13, and inconsistent lighting conditions caused by rapidly moving clouds when data for SNOW21:March was collected contributed to areas of very high error values within produced DEMs; error values as high as 2.16 m were found where dark shadowing was present, which effected ~ 31 % of the survey area. Validation points that fell within the problematic distorted and shadowed areas were removed prior to the elimination of outlier. However, where lighting was sufficient, error values were similar to those found in SNOW21:April (Table 4). As shown in Figure 13, the many problematic areas are concentrated near the centre and edges of the study plot, and appear as overestimations and underestimations of RPAS SD. Pixels covering 84,817 m^2 in SNOW21:March were removed prior to further processing decribed below.

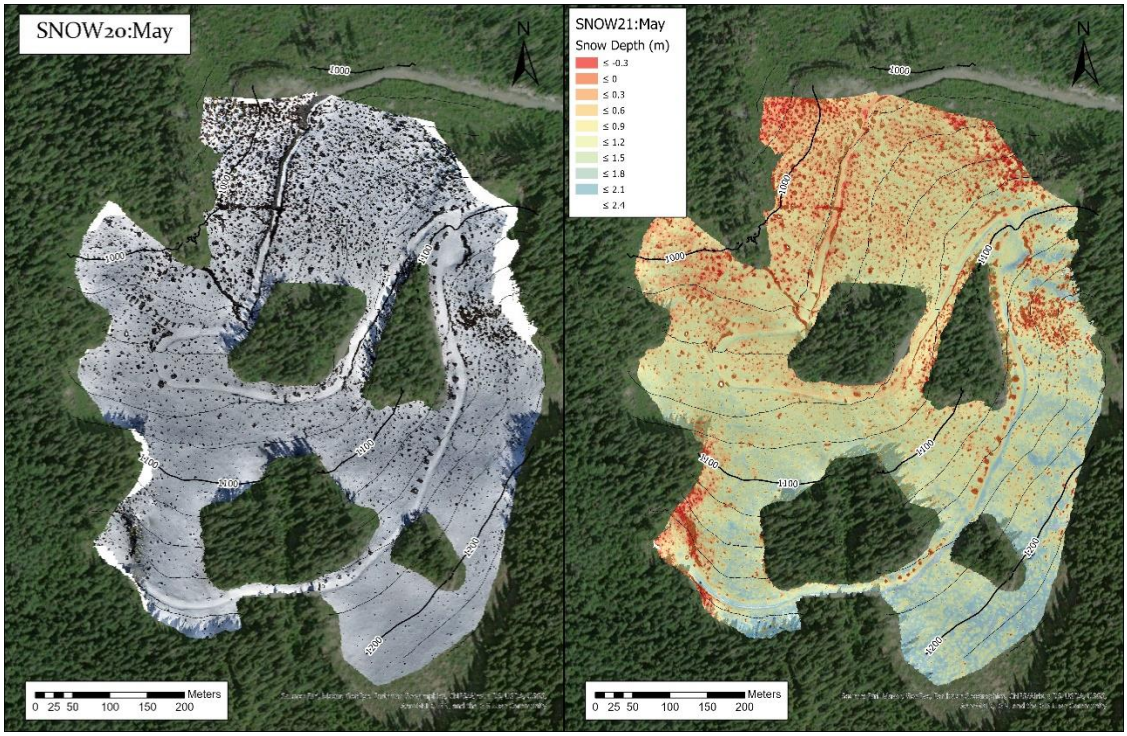

Figure 12. SNOW20:May orthophotograph (left) and RPAS SD Map (right) overlaid on satellite image

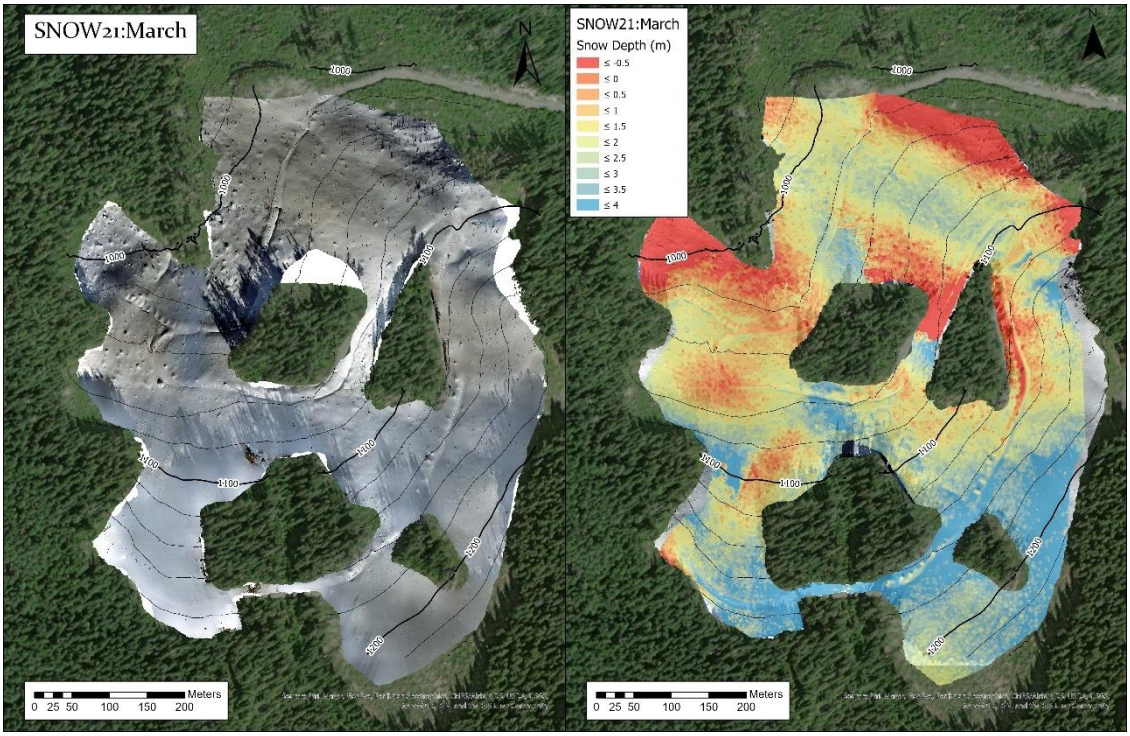

Figure 13. SNOW21:March orthophotograph (left) and RPAS Snow Map before problem areas were removed (right) overlaid on satellite imagery.

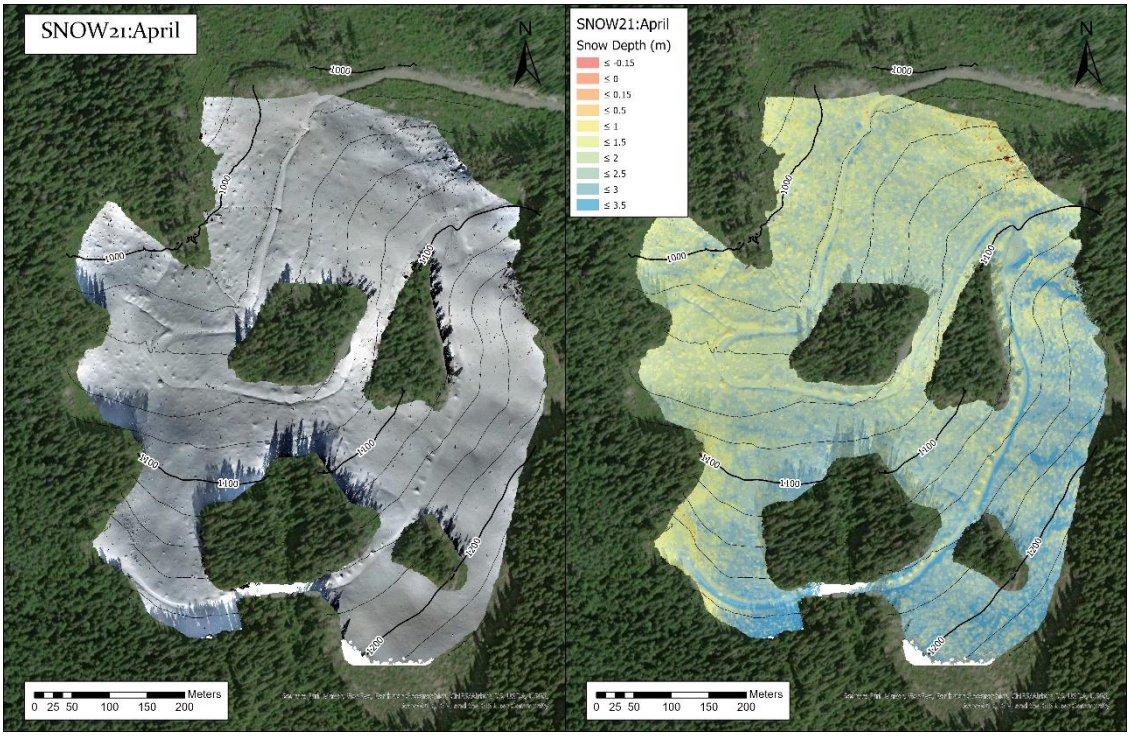

Figure 14. SNOW21:April orthophotograph (left) and RPAS SD Map (right) overlaid on satellite imagery.

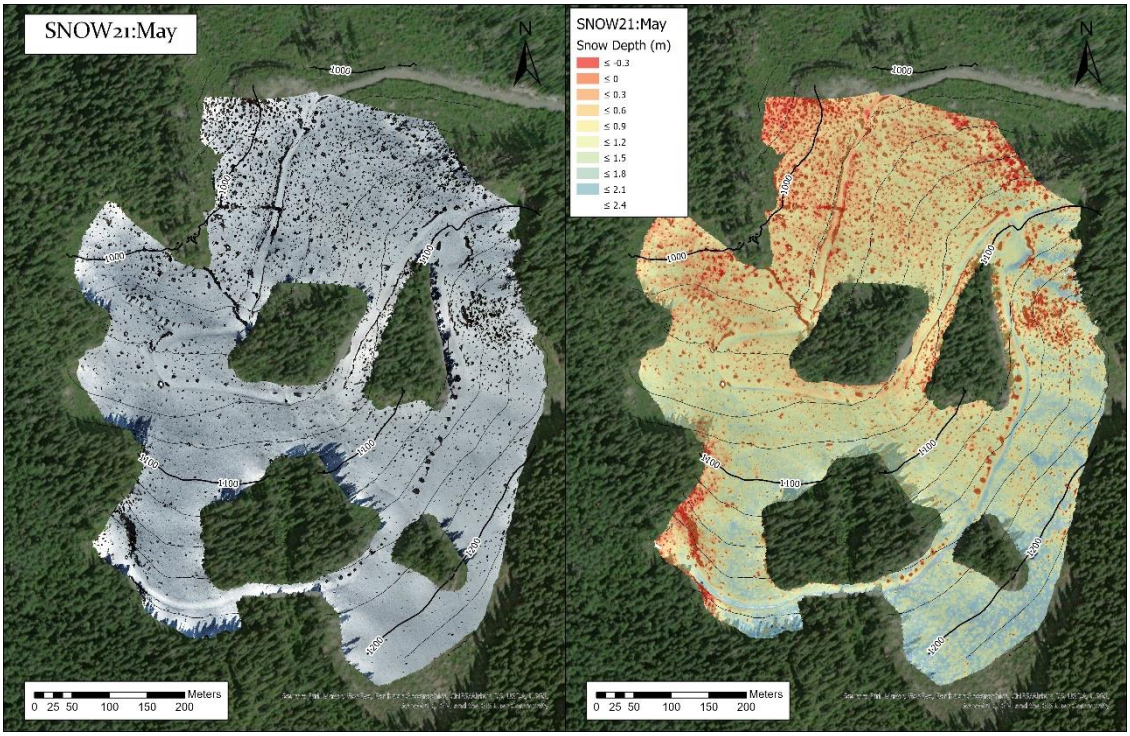

Figure 15. SNOW21:May orthophotograph (left) and RPAS snow depth Map (right)overlaid on satellite imagery.

4.4.1 RPAS SD Estimates: Road

On road sections throughout much of the study plot, many points have close agreement within ~ 0.10 m between validation and RPAS-SfM SD estimates, with best agreement found in SNOW21:May when 58 of 87 validation points fell in that range. On road sections in SNOW21:May, the RMSE was 0.08 m, with a MAE of 0.08 m, and MRE of 9.0 %, while in SNOW21:April, RMSE was 0.15 m, with a MAE of 0.14 m, and MRE of 7.0% . In SNOW21:March, the initial RMSE was 0.83 m for road validation points due to the heavy shadowing noted above. When validation points from shadowed sections were removed, RMSE for validation points on roads was reduced to 0.30 m, with MAE at 0.27 m, and a MRE of 18.0 % (Table 4).

Along road sections, SD was less variable than in surrounding off-road areas (Figure 17). Greatest depths on roads where found in the upper portions of the study plot near the upper weather station, possibly due to large trees that block solar radiation and wind, while in the NE and NW sections of the study plot, depths were shallower and more variable due to greater exposure to solar radiation and turbulent energy fluxes related to wind. In these locations, bare earth was extensive during the two melt period surveys conducted in May 2020 and 2021. In the immediate vicinity of road edges, high error values of up to 0.50 m were found in ditches on validation transects positioned across roads. Adjacent to such locations, error was in the typical range of ~ 0.02 - 0.10 m on roads, and ~ 0.05 m – 0.20 m off-road.

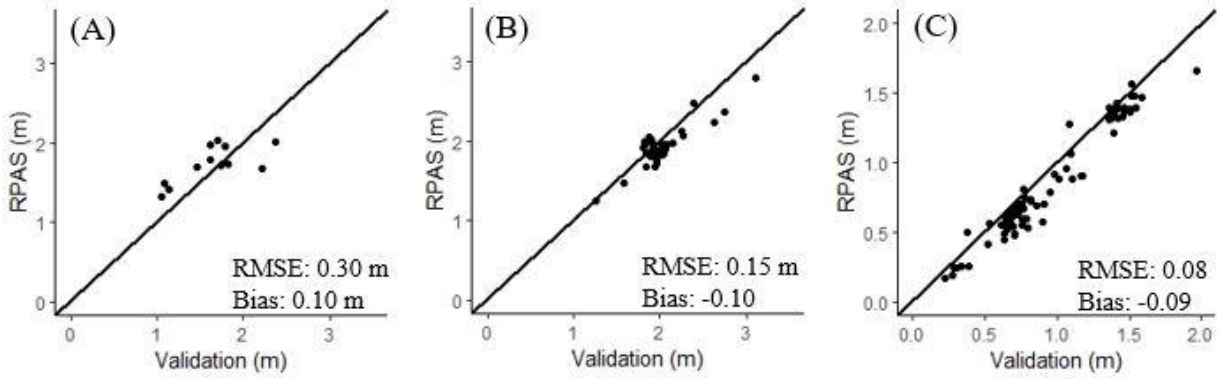

Figure 16. Scatter plots of RPAS SD estimates vs. on road validation point measurements. (A) SNOW21:MARCH, (B) SNOW21:APRIL, (C) SNOW21:May

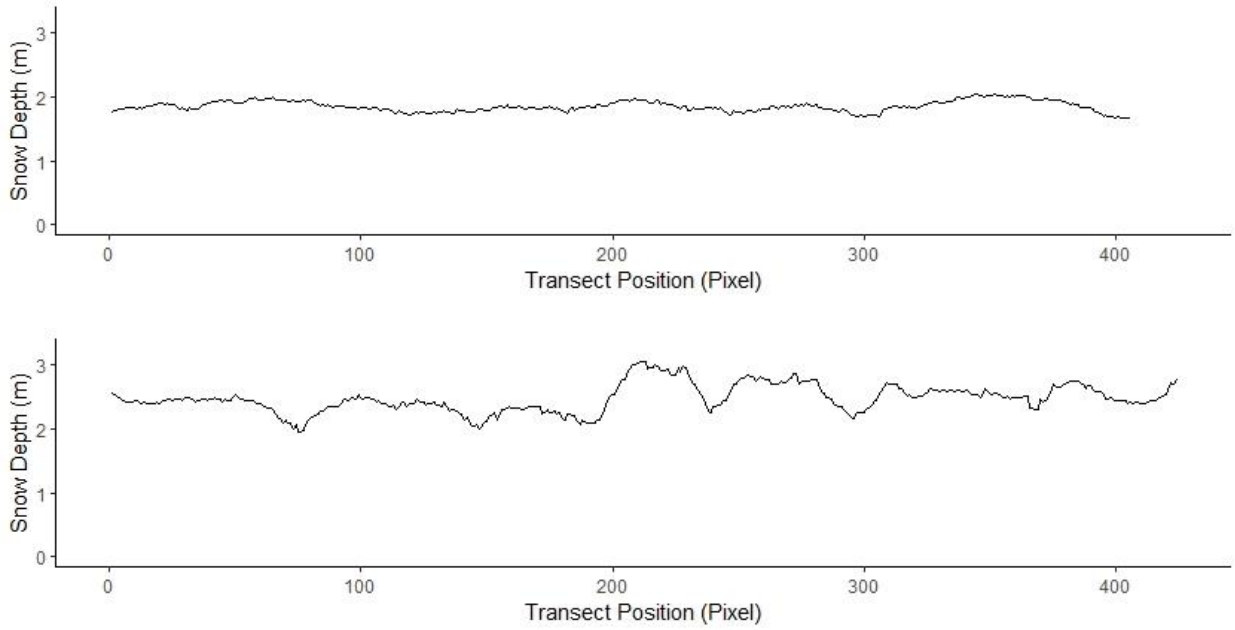

Figure 17. Cross sectional transects of RPAS SD estimation values along adjacent 80 m lines in SNOW21:April: The smoother top graph is on a road, and the bottom graph is from an off-road area directly above the road transect.

4.4.2 RPAS SD Estimates: Off-Road

Off-road portions of the study plot returned varying levels of accuracy, with RMSE values ranging from 0.36 m in SNOW21:May, and up to 0.59 m in SNOW21:April (Table 4; Figures 11 & 16). During the peak snowpack period in March and April, despite MAE values of up to 0.48 m, MRE of 17 % in SNOW21:March and 18% in SNOW21:April was found (Table 4). With lower SD in the two late spring snow surveys conducted in May of each field season, MRE was 29 % and 26 % in SNOW20:May and SNOW21:May respectively, while MAE was 0.32 m for both, with similar RMSE of 0.38 m and 0.36 m. Negative values are present in DEM outputs in the lower elevations areas of both SNOW20:May and SNOW21:May (Figures 12 &

15). Many of these negative values are positioned on stumps, small trees, and areas where full ablation had occurred. However, some areas with snow present also showed as negative.

4.4.3 Application of Offsets to Vegetated Off-Road Areas

In bare earth DEMs, the thick perennial vegetation that covers 73% of the study plots was misclassified as the ground. Because the winter snowpack compressed vegetation, widespread negative bias occurred when misclassified vegetation rebounded in bare earth DEMs, producing erroneous positive biased elevation values. When the snow melts, the vegetation rebounded by up to and over 1 m as noted above in section 5.1.0. Because RPAS-SfM is incapable of penetrating to the ground through dense vegetation, and removing it from the surface model is impractical due to its wide extent and density, positive offsets were applied to vegetated portions of DEMs to address the extensive negative bias found in SD outputs.

Offset values were selected by iteratively determining the value that produced the lowest MAE for each dataset (Table 5). Selected offset values were close to the bias of each dataset (Table 5). Offsets were applied to areas classified as vegetation by the supervised classification, which had a calculated accuracy of 86.3 % as determined by 200 stratified random points in the accuracy assessment (Figure 18). This method reduced MRE to under 15% in off-road areas in all 2021 datasets, and from 29% to 21% in SNOW20:May, while shifting biases to -0.10 m and -0.9 m that had ranged from -0.25 to -0.46 m in all surveys except SNOW21:March, which was shifted from -0.31 to -0.14 m (Table 5). Most negative values visible in DEM outputs shifted to positive, while exposed vegetation that had rebounded from under the snow surface was correctly left as negative (Figures 18 & 19).

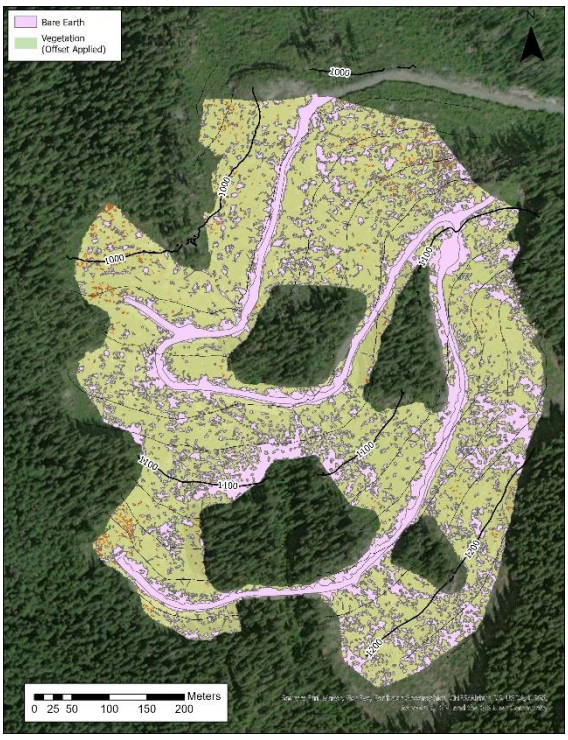

Figure 18. The study plot divided into vegetated and non-vegetated areas by a supervised classification process. Areas classified as vegetated have offsets applied to them.

Table 5. Error metrics for vegetated off-road areas with, and without, offsets.

Dataset	Terrain Type	Number of SD Validation points	Offset (m)	Bias (m)	MAE (m)	MRE (%)	RMSE (m)
SNOW20:May	Off Road	173	n/a	-0.25	0.32	29	0.38
SNOW20:May	Off Road - Offset	173	0.26	-0.09	0.22	21	0.28
SNOW21:March	Off Road	41	n/a	-0.31	0.39	17	0.45
SNOW21:March	Off Road - Offset	41	0.28	-0.14	0.31	14	0.37
SNOW21:April	Off Road	60	n/a	-0.46	0.50	19	0.59
SNOW21:April	Off Road - Offset	60	0.48	-0.09	0.26	11	0.32
SNOW21:May	Off Road	59	n/a	-0.31	0.32	26	0.36
SNOW21:May	Off Road - Offset	59	0.28	-0.10	0.15	15	0.18

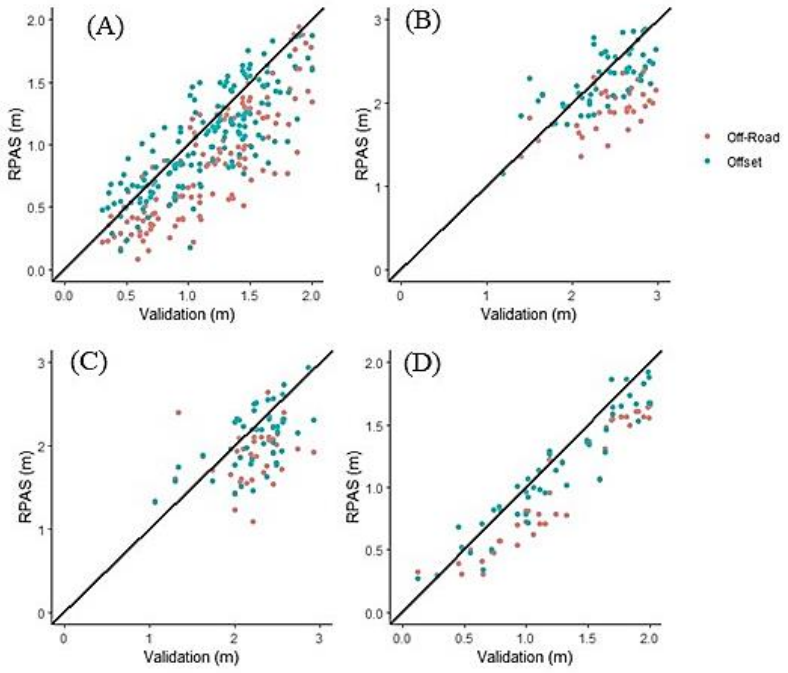

Figure 19. Scatterplots of off-road RPAS estimates vs. validation measurements, with and without offsets applied. (a) SNOW20:MAY, (b) SNOW21:MARCH, (c) SNOW21:APRIL, (d) SNOW21:MAY

Before calculating SWE and stored water estimates, negative values that remained were set to zero, while excessively high values located primarily near DEM edges that were greater than 5 m during peak snowpack, and 3 m during the melt period were set to 5 m and 3 m respectively. These cut-offs were selected as the only pixels containing values greater than 5 m at peak snowpack, and 3 m during the melt period were found on the edge of DEMs where outliers caused by doming are typical (Girod & Filhol, 2020). During peak snowpack, MRE of RPAS SD models was below ~ 15% across most of the lower elevation portions of the study plot, and ~ 10% or lower throughout the upper portions when offsets were applied. On roads and bare areas where offsets are not applied, we see MRE of under ~ 5% throughout. Similarly, during late spring snow conditions, MRE is greater in lower elevation areas where SD is lower. Offsets were

not applied to road and bare sections as the bias seen (-0.09 m, -0.10 m, 0.10 m) falls within the range where it cannot be differentiated from noise within DEMs as error adds up when conducting terrian differencing (Harder et al., 2016).

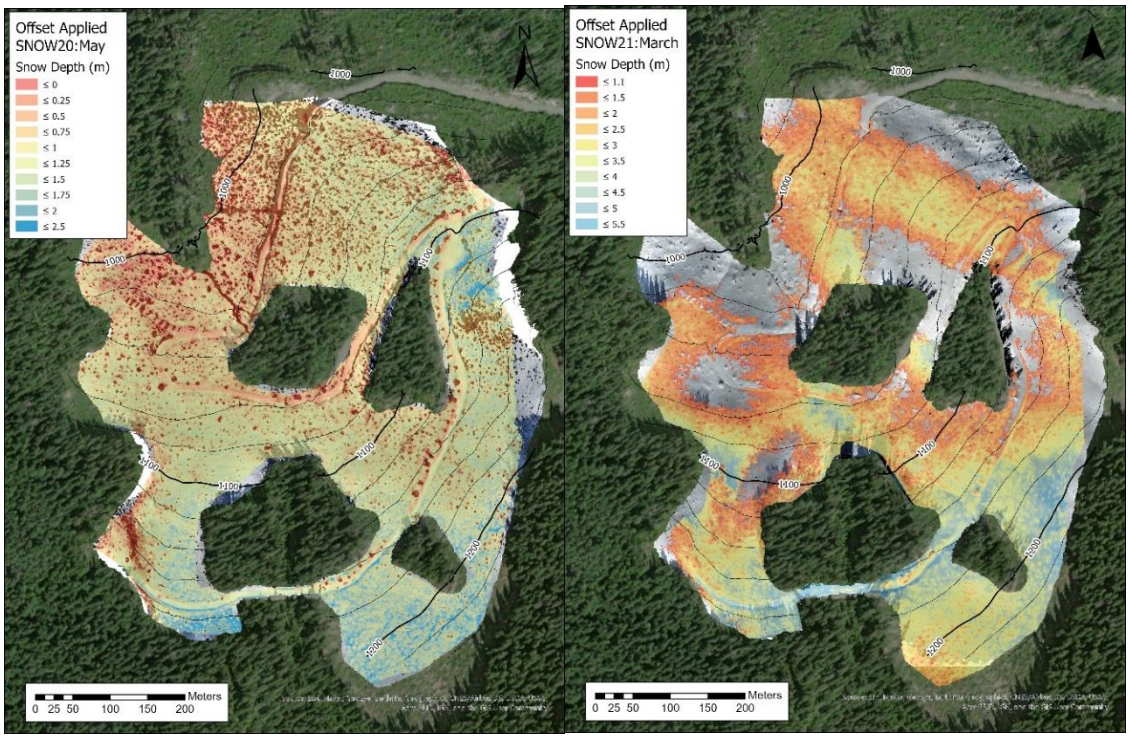

Figure 20. Remotely Piloted Aircraft System snow depth estimates with offsets applied. SNOW20:May (left) SNOW21:March with problematic shadowed areas removed (right)

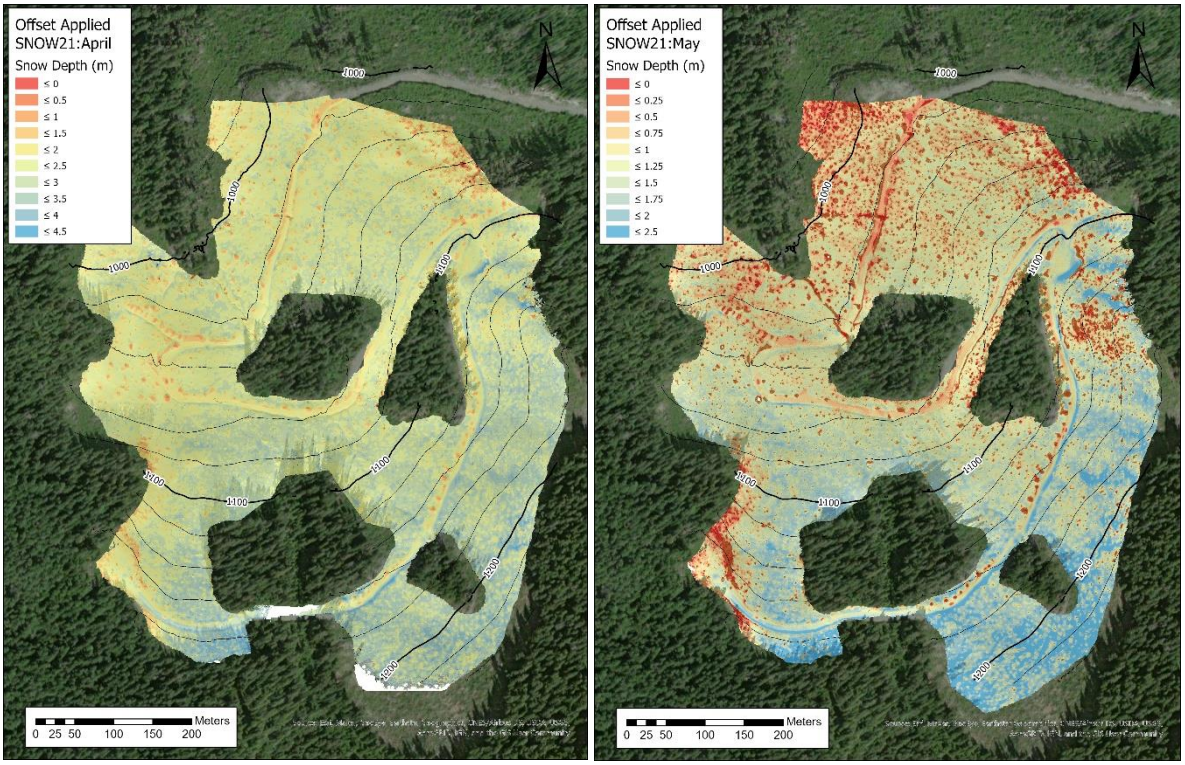

Figure 21. Remotely Piloted Aircraft System- Structure from Motion snow depth estimates with offsets applied. SNOW21:April (left) SNOW21:May (right)

4.5 SWE Results

4.5.1 Manual SWE Measurements

The number of SWE measurements collected throughout the field campaigns varied from 55 in SNOW20:May to only 10 in SNOW21:March (Table 8). Mean SWE values ranged from a high of 766 mm with a standard deviation of 188 mm in SNOW21:April, to a mean low of 475 mm with a standard deviation of 155 mm in SNOW20:May (Table 6). As with SD, manually measured SWE values were relatively homogenous across the study plot during peak snowpack, though consistently greater at higher elevations, with much greater variation in late spring as exposure to wind and solar radiation, and varying slope angles and aspect resulted in differing melt rates.

Snow density was generally consistent across the study area during each survey, particularly in late spring. Throughout the spring, mean density increased from 322 kg/m^3 with a standard deviation of 37 kg/m^3 in SNOW21:March to 434 kg/m^3 with a standard deviation of 46 kg/m^3 during SNOW21:May (Table 6). In SNOW21:March, density was greatest at higher elevations, while later in the spring as melt progressed, snow density was greater in the westerly, lower elevation portions of the study plot.

4.5.2 RPAS Derived SWE Estimates

Deriving SWE from RPAS-SfM derived SD values across the study plot was done by first calculating the mean snow density for each dataset using manually measured SWE values. Next, bias corrected SD DEMs were multiplied by the mean snow density from each field visit, which created DEMs of estimated SWE. Being derived from SD DEMs, SWE pixel values extracted at validation points show a similar pattern to that of RPAS-SfM SD estimates, with the lowest error values being found on road sections (Table 6). The lowest overall error levels for SWE estimates were found in SNOW21:April with a RMSE of 94 mm, MAE of 57 mm, and MRE of 10.2 % (Table 6). MRE varied from 8.9 % on road sections of SNOW21:April, and up to 29.6 % in SNOW20:May, which consisted of only off-road manual SWE measurements. MAE varied from a low of 41 mm on road sections in SNOW21:March, to a high of 126 mm in off-road sections of SNOW21:April. Because derived SWE values were calculated from SD DEMs, and the mean of manually measured snow density, SWE distribution shown on maps appears essentially the same as SD maps above, and are therefore not presented here.

Table 6. Snow density measurements, mean validation SWE values and mean RPAS-SfM values at validation points, and error metrics of validation SWE and RPAS-SfM derived SWE differences.

Survey ID	Terrain Type	N=	Mean density (kg/m3)	Density Std Dev (kg/m3)	Mean Validation (mm)	Mean SfM (mm)	Validation Std Deviation	SfM Std Deviation	MAE (mm)	MRE (%)	RMSE (mm)
SNOW20 :May	All	54	416	107	491	408	146	195	112	29.6	140
SNOW21 :March	Road	10	322	45	431	343	47	11	41	19.4	96
SNOW21 :April	All	15	369	34	697	653	212	165	75	10.2	94
SNOW21 :April	Road	10	367	37	559	540	62	14	50	8.9	59
SNOW21 :April	Off-Road	5	370	17	973	879	113	66	126	12.7	140
SNOW21 :May	All	20	434	42	613	576	85	117	84	13.8	427
SNOW21 :May	Road	12	468	31	627	571	55	35	68	10.6	290
SNOW21 :May	Off-Road	8	423	43	592	582	113	179	107	18.5	313

At the two weather stations where regular snow courses are conducted as part of a long-term monitoring program, close agreement between manually measured and SfM-derived SWE values was found. Snow course measurements across all datasets that overlapped with SfM DEMs (n=26) had a mean of 550 mm and standard deviation of 87 mm, while SfM-derived SWE had a mean of 502 mm and standard deviation of 91 mm. MAE and MRE of differences between all SfM-derived and manual snow course SWE was 64 mm and 11.9 %. Best results were found in SNOW21:April and SNOW21:May with a MAE of 65 mm and 50 mm, and MRE of 8.9 % and 10.5 % respectively. In SNOW21:March, where only 6 SfM-derived measurements where attained at the lower weather station, MAE was 87 mm, and MRE was 19 %; these measurements bordered an area with unreliable DEM results as detailed in Section 5.2.1 above. In the vicinity of the upper weather station, distortion and noise from adjacent forest stands prevented SfM SWE retrieval at the snow course location during SNOW21:March and SNOW21:April. At the lower weather station, SfM derived SWE did overlap with snow courses during these surveys. However, this part of the study plot routinely has less snow than the

surrounding landscape. SWE measured at the Mt. Cain automated weather was much higher than the mean of manual measurements and SfM SWE recorded at this lower station. However, in SNOW21:May, the mean of manual measurements and SfM SWE recorded at the upper weather station are in close agreement to the SWE measured at Mt. Cain (Table 6). No snow course data was available for SNOW20:May.

Table 6. Manual vs. RPAS-SfM derived SWE at weather station (Wx) snow course locations.

Survey ID	Location	n=	Mean Validation SWE (mm)	Validation Std Deviation (mm)	Mean SfM SWE (mm)	SfM Std Deviation (mm)	MAE (mm)	MRE (%)	Mt Cain SWE Sensor (mm)
SNOW21:March	Lower Wx	6	431	47	343	11	87	19.4	979
SNOW21:April	Lower Wx	10	559	62	539	14	50	8.9	1052
SNOW21:May	Upper Wx	10	613	43	563	29	65	10.5	615

4.6 Snow Depth and Distribution

Calculated from up to and over 5,000,000 SD pixel values per survey across an area of 283,739 m^2, the mean SD of DEMs with offsets applied across the study plot ranged from 0.91 m in SNOW20:May to 2.49 m in SNOW21:March, with standard deviations ranging form 0.47 m to 1.00 m respectively (Figure 22). Earlier in the snow season, SD was fairly homogeneous across the study area, however, once melt began in the spring, variation across the study plot increased as SD decreased rapidly at lower elevations, and on open slopes exposed to sun and wind, exposing wide areas of bare earth and reducing SD to under 1 m in large, while much of the upper study area remained covered with up to 2.5 m of snow (Figure 12-15, 22). During the peak snowpack period shown in SNOW21:March and SNOW21:April, only trees, logs protruding from slash piles, and a stream were exposed above the snow surface (Figures 13 &

14). In RPAS-SfM SD distributions shown in Figure 22, relatively normal distributions is seen in three of the four datasets; note the distribution of SNOW21:March is corrupted by high error values, and the removal of erroneous pixels that existed in shadowed areas.

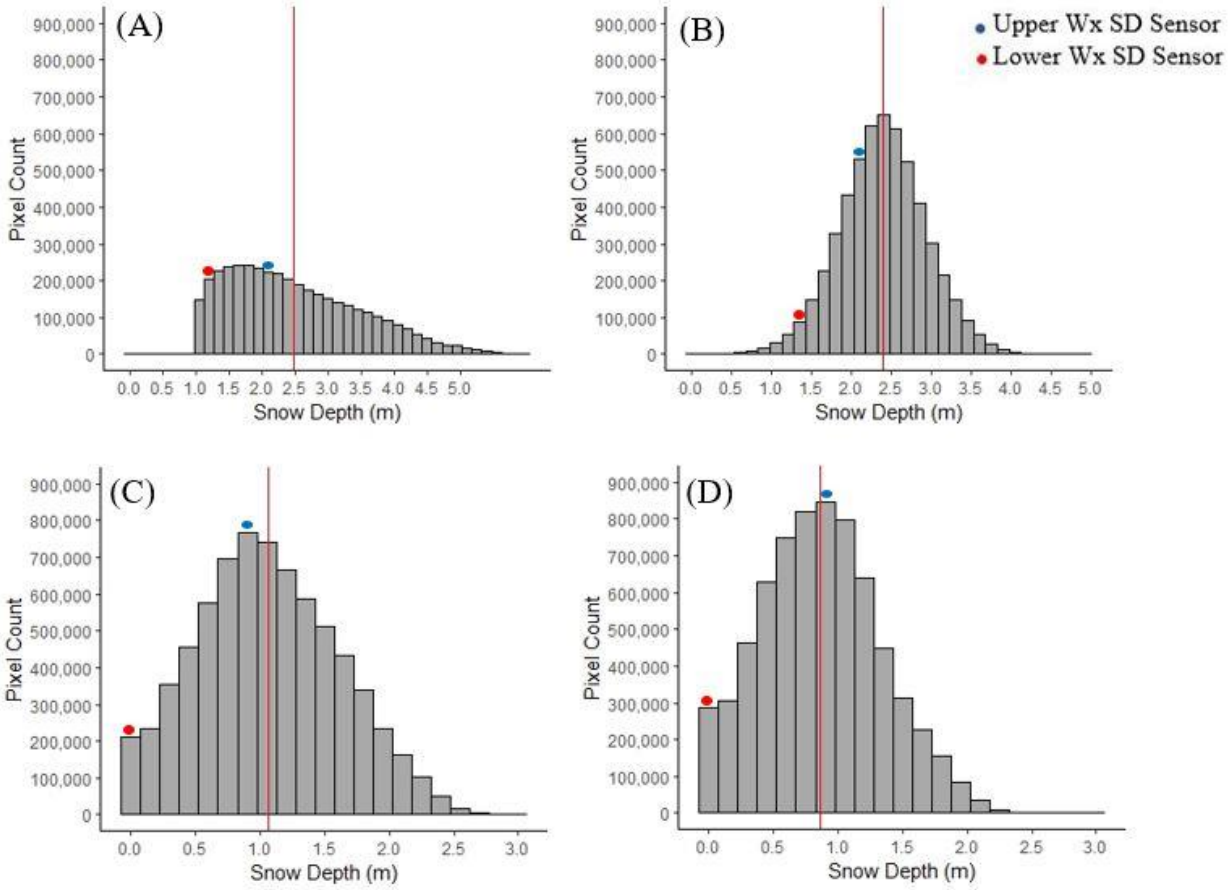

Figure 22. (A) SNOW21:March, (B) SNOW21:April, (C) SNOW21:May, (D) SNOW20:May. Snow depth distribution across all RPAS-DEMs, with mean (red line). Note that SNOW21:March is skewed due to error caused by deep shadowing and the removal of erroneous pixels in such areas.

The greatest SD values were found in generally northern facing higher elevation portions of the study plot, where solar radiation and wind is intercepted by forest stands. At the upper weather station during the 2019-2020 field season, from November 1st until March 10th when peak snowpack was recorded by the SD sensor, a total of 51,965 W/m^2 of solar radiation was recorded, while at the lower station, 106,095 W/m^2 was observed. During the melt period from

March 10th – May 31st, similar amounts of solar radiation were observed at both stations with 306,177 W/m^2 at the upper station, and 329,944 W/m^2 at the lower station, however, during both the accumulation and melt periods, much greater winds speeds with a mean of 6.20 m/s and 5.74 m/s were recorded at the lower station compared to a mean of just 0.73 m/s throughout the snow season at the upper station. The much stronger winds observed at the lower station, coupled with greater amounts of solar radiation led to higher melt rates than in the upper study plot. Strong winds also caused road banks and shallow gully features along the steep and open eastern edge of the study plot to accumulate significantly more snow than surrounding areas (Figures 12-15)**.** In both May surveys, throughout the lower and mid sections of the study plot, stumps, slash piles, sections of road, road cuts, and downhill road fill areas were snow free. Upper portions of the study plot remained largely snow covered, with exposed stumps scattered throughout. Deeper snow was found in areas shaded by forest, in shallow gully features, and on uphill portions of roads. Stumps and slash piles were associated with increased melt rates, with rings of exposed ground observed around such features (Figures 13 & 15). During SNOW21:May, in addition to the snow surface being covered in sun cups, surface rilling was visible in the steep SE section, which may have been caused by rainfall or melt water running down the snow surface.

The distribution of manual SD measurement captured the range of depths shown by the SfM-SD distribution in May of both field seasons, however, during peak snowpack, deeper SD captured by SfM outputs was missed by manual measurements (Figure 22 & Figure 23). The mean of RPAS-SfM SD and manual SD measurements in SNOW21:April and SNOW21:May are within 0.13 and 0.03 m respectively of each other, but diverge in SNOW20:May and SNOW21:March at 0.32 m and 0.31 m. The SD recorded at the upper weather station was within

0.15 m of validation means in all field campaigns except SNOW20:May, when they diverged by 0.34 m. Standard deviation of validation points in all datasets ranged by just 0.04 m, from 0.43 – 0.47 m.

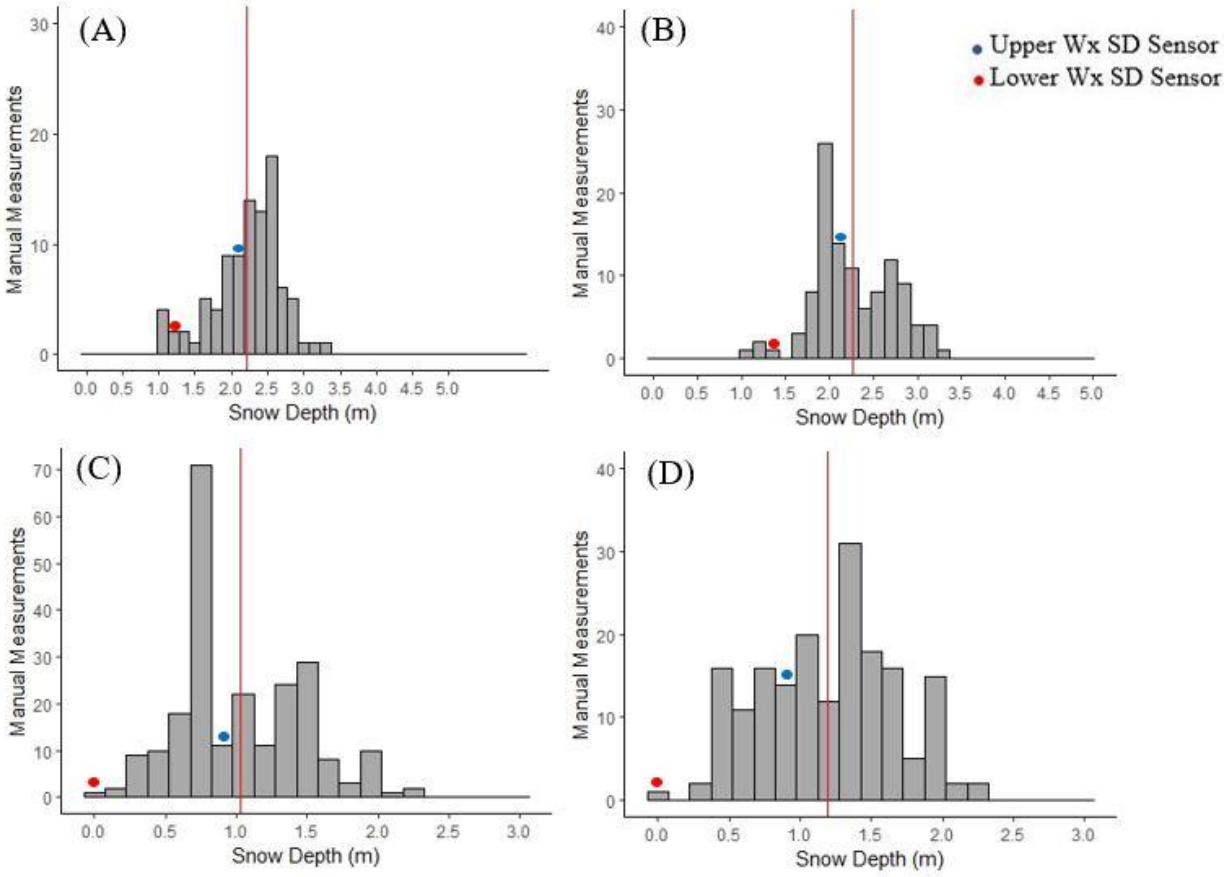

Figure 23. (A) SNOW21:March, (B) SNOW21:April, (C) SNOW21:May, (D) SNOW20:May. Snow depth distribution of all manual validation points with the mean (red line) and weather station snow depths at the time of each survey.

4.7 Total Stored Water Estimates

During the 2021 field season, the greatest amount of stored water content recorded was in SNOW21:April, which was collected 5 days prior to the peak SD recorded on April 10th by the onsite automated weather stations; SWE at the Mt. Cain weather station also peaked on April 10th. Between SNOW21:April and the next survey on May 14th (SNOW21:May), daytime

temperatures of up to 15°C occurred, and below freezing temperature occurred only 20 % of time (Figure 9). As recorded at the lower weather station, these warm conditions were accompanied by an average wind speed of 5.1 m/s, and spikes in solar input that reached over 750 w/m^2 throughout that period. Together, these conditions caused depths to plummet by over 1 m at both the upper and lower weather stations. In a little over a month, total estimates of total stored water decreased by 48 %, dropping from 245,700 m^3 on April 5th, to 119,201 m^3 on May 14th. During the same period, SD and stored water shifted from being generally homogenous across the study plot to being concentrated at higher elevations in SNOW21:May (Figure 25). Part of this shift can also be attributed to the greater amount of higher elevation area in the study plot consisting of northerly facing slopes that are adjacent to forest stands where solar and wind induced melt has less impact.

During peak snowpack, the distribution of stored water was close to even by aspect; 54.1 % of stored water was found on the northerly slopes that account for 54.0 % of the study plot, while 42.6 % was stored on westerly slopes that make up 42.0 % of the area. When melt was well underway in SNOW20:May and SNOW21:MAY, stored water shifted further to northerly slopes, at 56.9 % and 58.9 % respectively (Figure 22). Minimal area consists of easterly and southerly aspects within the study plot.

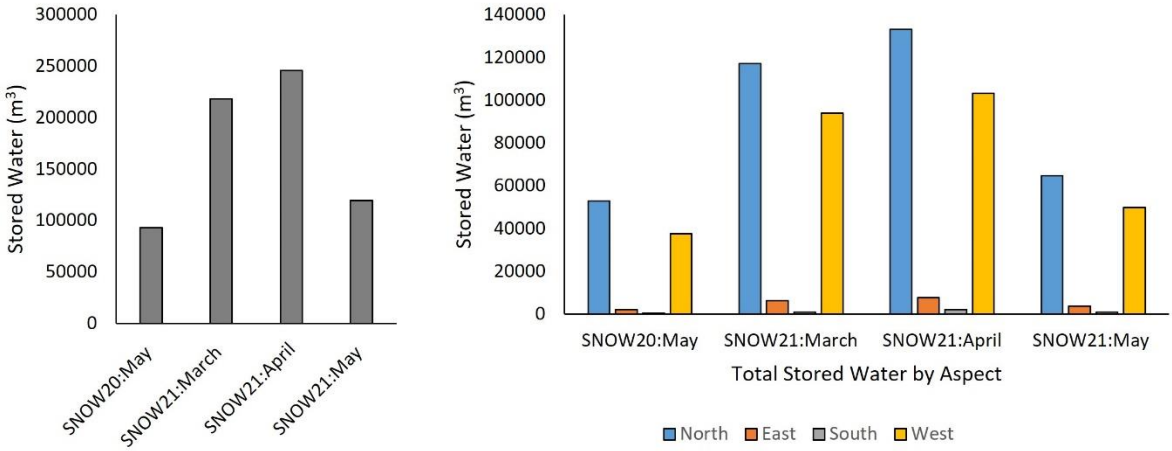

Figure 24. Estimated total water stored as snow (left) and estimated water stored by aspect (right).

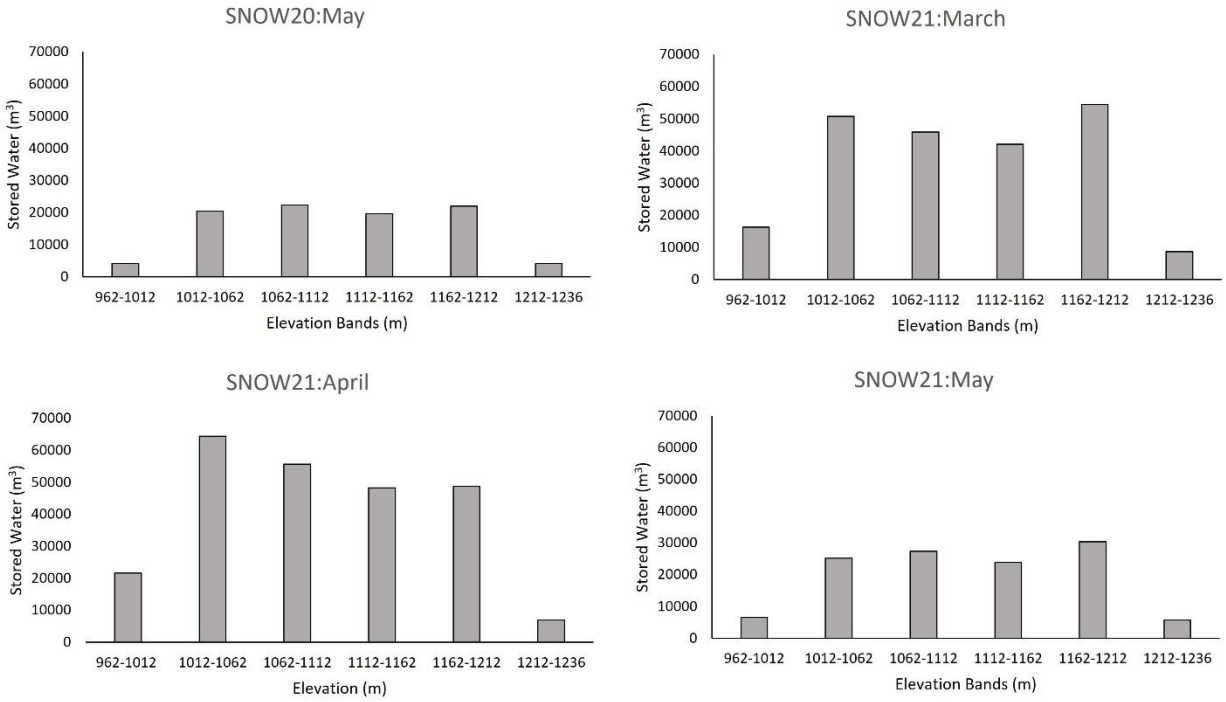

Figure 25. Estimated water stored as snow by elevation bands and field campaigns. Note: The final SNOW21:March DEM contains less area due to the removal of erroneous pixels, therefore, to match the other surveys, water volume values have been adjusted by multiplying the mean stored water value of each m2 by the area of elevation bands before the erroneous pixels had been removed.

The greatest concentration of water was stored at higher elevations, particularly in May after warm stretches during April of both field seasons resulted in rapid melt as shown in (Figures 8, 9, & 25). In SNOW21:April, which was conducted 5 days prior to the peak SD recorded at the automated weather stations, the three lower elevation bands which account for 62 % of the study plot held 58 % of stored water. Despite the upper three elevation bands accounting for only 38 % of the study plot area, by SNOW21:May, stored water was essentially evenly split between upper and lower portions of the study plot (Figure 25).

4.8 Discussion

4.8.1 RPAS SD Estimates in Disturbed Vegetated Terrain

This study used RPAS-SfM methods to map and estimate SD and SWE in a 52 ha cutblock that was harvested in 2008. On road surfaces and other unvegetated areas of the study plot, accuracy of RPAS-SfM SD estimates produced across varying snow and illumination conditions were within the 0.06 m – 0.30 m RMSE range of previous studies that examined open, mostly unvegetated areas (Avanzi et al., 2018; Bühler et al., 2016; Harder et al., 2020). Excluding the problematic SNOW21:March survey, the application of positive offsets to vegetated off-road area improved accuracy of all areas to within the range of the previous studies noted above. Resultant RMSE values align with previous studies that examined areas containing vegetation, such as in Bühler et al., (2016) where RMSE of 0.15 m and 0.30 m was found in two separate plots that contained primary low grass with some shrubs, and the RMSE of 0.19 m reported within shrubby areas in Harder et al., (2020).

In May of both field seasons, longer spring days and higher sun angle offered the best lighting for RPAS-SfM surveys, with minimal shadowing. The snow surface had well developed

melt patterns, and was covered in forest litter. Additionally, extensive areas of exposed bare earth and logging debris were protruding from the snowpack, all of which contributed to enhanced contrast, favoring increased point detection and alignment of DEMs across both snow and bare earth surfaces (Gindraux et al., 2017).These ideal snow surface and lighting conditions that were aided by bare earth patches resulted in SfM outputs with the best snow surface DEM results of this study at RMSE 0.083 m in SNOW21:May, which aligns with previous studies examining mountainous terrain (Bühler et al., 2016; Cimoli et al., 2017; Harder et al., 2016). The bare earth DEM used for SD calculations had a RMSE of 0.013 m, which falls within the lower range of previous works using RPAS-SfM to map snow surfaces in mountainous terrian (eg. Bühler et al., 2016; Harder et al., 2016; Revuelto., et al., 2021).

Conversely, the fresh snow surface, as well as variable lighting conditions caused by intermittent cloud during SNOW21:March led to far less point matches and lower accuracy results, which agrees with the findings of Bühler et al (2017) where errors of over 1 m existed in similar conditions. Further, low sun angle during the same survey casted long shadows from forest stands, which caused very poor results in affected areas. However, in non-shadowed areas, error values were similar to SNOW21:April when minimal shadowing was present, but snow conditions were similar. These findings agree with Bühler et al (2017) where deep shadowing also caused widespread errors >1 m was experienced. As reported in Bühler et al (2017) and further confirmed here, using RPAS-SfM methods to estimate SD where deep shadowing exists can result is very high error values, and therefore should be avoided.

4.8.2 DEM SD Variation

RPAS-SfM has introduced a flexible and low-cost way to estimate SD at high resolutions across a landscape at very high spatial resolutions, which allows examination of surface patterns and textures. Here**,** the creation of orthophotos with 2.5 cm resolution allowed fine scale visual examination of the snow surface. A variety of different snow patterns and textures created by wind and melt are visible within the orthophotographs, such as sastrugi, ripples, pillows, and scouring created by wind, and snow surface melt patterns such as suncups and snow surface rilling.

Throughout the study plot, small scale SD variation is highly visible within RPAS-SfM outputs. Highlights of such variability includes areas of deep snow in ditches, gully features, and higher elevation areas, as well as shallower snow on the downhill sides of roads, and lower elevation areas (Figures 20 & 21). Stumps throughout the study plot are visible as circles of shallower SD during peak snowpack in SNOW21:March and SNOW21:April, and as very shallow or snow-free areas during the melt period in SNOW20:May and SNOW21:May (Figures 20 & 21). The volume of these accumulation and melt patterns are quantified in SD DEMs. Such variations in SD, which vary much more than density, are likely missed by current observation networks, both at broad scales, and nearby weather stations. The ability of RPAS-SfM to produce outputs that show such snow structures offers a powerful new tool that can be used to advance research in snow distribution and melt dynamics.

A research topic that could be addressed using RPAS-SfM is the relationship between the height of stumps left behind by logging operations and the snow accumulation and melt dynamics surrounding them. Within outputs from both May surveys, it is evident that there is

enhanced snow melt surrounding the many tall stumps found within the study plot. As soon as the dark surface of the stumps becomes exposed to solar radiation, much more solar energy will be absorbed than the surrounding snow surface, which will then radiate out to the snow around them (Harder et al., 2017). Quantifying this relationship could provide useful information that could be used to reduce the impacts that logging can have on the hydrology of watersheds. Similarly, research into local-scale advection from exposed ground such as discussed in Harder et al., (2017) could be further explored and expanded to larger areas using RPAS-SfM outputs. Other research topics that could be explored using the ability of RPAS-SfM to show small-scale SD variability include avalanche dynamics, wind transport of snow, impacts of rain-on-snow events, and more.

4.8.3 Error

While RMSE is the standard metric referred to when evaluating error in this discipline, MRE is another important measure to consider when assessing the use of RPAS-SfM to estimate SD. Due to the typically deep winter snowpack found within the region this study took place, MRE can be low despite the sometimes high MAE of over 0.20 m that was found in some areas of the study plot. While not a problem in the two snow seasons examined in this study, during unseasonably low snow seasons, or in regions where SD is typically low, error and bias may come close to, or surpass SD in terrain containing thick vegetation and open terrain alike as was seen in Lendzioch et al. (2019). Because the error in DEMs produced using RPAS-SfM methods over snow surfaces is rarely below 0.10 m, and is additive when combining two DEMs during terrain differencing, Harder et al. (2016) state that it is currently impractical to estimate SD using these methods where snow is under 0.30 m as error may be greater than the actual SD. This is

especially true in complex terrain such as was examined in this study. With best case results within vegetated areas in this study still containing a MAE of 0.15 m, and up to 0.31 m, attempting to measure areas of shallow snow below ~ 0.30 m where vegetation is present results in high MRE, with error greater than measured SD found in some studies. In this study, the few validations (n= 7) that were under 0.30 m had relative error that varied from 4 – 171 %.

4.8.4 Impacts of Vegetation and Offsets

Tall perennial shrubs and small trees cover much of the area examined here, and were the primary source of SD DEM error in off-road sections. Once the snowpack forms, the perennial shrubby vegetation is pressed almost completely flat against the ground; digging ~ 3 m down to the bottom of the mid-winter snowpack exposed shrubby vegetation no more than ~ 0.05 m off of the ground, while small trees were seen bent downhill, but not flat against the ground (Figure 26). Upon ablation, these shrubs and small trees rebounded, and quickly begin to grow new foliage. The thick nature of this vegetation caused the SfM process to identify the top of shrubs that blanket much of the study plot as the ground surface (Figure 26).

Figure 26. Thick, ground covering vegetation blanketing the study plot (left). Vegetation pressed tightly against the ground under the snowpack (middle). Small trees and shrubs rebounding as the snowpack melts (right)

Within the existing literature of RPAS-SfM SD estimations, most vegetation described is sparser, or in patches. Approaches used to resolve the issue of negative values have included setting SD in problematic vegetated areas to zero (Buhler et al, 2016), or to the lowest manually measured SD values (Lendzioch et al., 2016); these approaches are impractical in this study due to the almost complete extent of vegetation cover. Instead, the application of positive offsets to vegetated areas within DEMs was found to reduce error levels where a systematic negative bias was found. While negative bias of -0.09 to – 0.10 m was found on road section in three or the four field campaigns, this could be considered noise as a certain amount of additive error is unavoidable when conducting terrain differencing (Harder et al., 2016), therefore, applying offsets to areas with already minimal bias may only add further noise. However, in areas containing tall perennial vegetation, the application of positive offsets is a simple and effective method to help overcome consistent negative bias and associated error that is found when such vegetation rebounds after ablation of the snowpack. Offset values depend on the height of the

vegetation that is being misclassified as bare earth. To determine the ideal offset value, well distributed SD validation points are needed to capture the variation of bias and error. In simple terrian that contains vegetation with minimal height variation such as grass, it may be possible to determine offsets value from vegetation height measurements, thus reducing or eliminating the necessity of conducting widespread manual SD validations. However, to determine accuracy of SfM SD estimates, manual measurements are still needed.

4.8.5 Potential for Operationalized RPAS SD Mapping

Throughout the world, LiDAR has been used extensively to measure snowpack across a variety of landscapes, including for water resource management applications (e.g.. Deems et al., 2013; Ferraz et al., 2018; Harpold et al., 2014; Painter et al., 2016; Raleigh & Small, 2017). As highlighted in Harder et al. (2020), RPAS-SfM SD surveying is incompatible for measuring SD in forested areas with canopy closure, which was further confirmed here. SfM processing of heavily forested areas produced outputs with distorted results, and where the snow surface was visible within forested areas, change detection analysis returned extremely erroneous SD values, varying from -5 m and up to and over 20 m. To overcome this issue, RPAS-SfM SD estimates on the periphery of forest stands could be used in combination with manual under canopy measurements to interpolate SD and SWE within forest areas. While LiDAR can measure under the forest canopy where RPAS-SfM cannot, in open areas, neither approach can consistently penetrate through thick ground covering vegetation, leading to converging results and levels of error between these two methods (Harder et al., 2020); owing to far lower costs, and relative simplicity of data collection and post-processing, the use of RPAS-SfM methods can be seen as a more practical approach than using LiDAR to measure SD in open areas when shadowing and

low sun angle is not a concern. As highlighted by Broxton & van Leeuwen (2020), when coupled with aerial LiDAR outputs, RPAS-SfM outputs can work to extrapolate SD across much wider areas outside RPAS survey plots using previous LiDAR surveys. This approach could work well to expand RPAS-SfM based survey results across a watershed were LiDAR data has been collected, and be used for ongoing snowpack monitoring.

In this study, the installation of a permanent above-snow GCP network proved to save a significant amount of time during field campaigns, as well as during post-processing. With the permanent GCP network installed and already surveyed, field crews were able to commence RPAS flights almost immediately upon arrival to the field site, which was particularly beneficial on days when travel to the study plot was difficult and slow due to challenging snow conditions. Snow accumulation atop GCPs was minimal, while only two of the 18 GCPs were ever buried under the snow surface. When temporary GCPs were used, and manual measurement plots centre coordinates were being collected, having the known position to install the RTK GNSS unit on allowed previously collected base coordinates to be entered, meaning additional lengthy collection periods were unneeded, further speeding up surveys. The precision of coordinates collected across the GCP network met, or exceeded that of standard temporary GCPs.

In the province of BC where this study took place, snow monitoring is conducted using primarily automated weather stations, and monthly to bi-weekly snow courses. Within some watersheds that supply communities with drinking water, active logging takes place. With minimal additional staffing, methods developed in this study could be applied during field trips already taking place to service such weather stations. If a GCP network is installed, and coordinates are established, one field technician could conduct RPAS flights while others do

standard weather station servicing, as well as snow courses. SWE measurements collected in snow courses can work to supply mean snow density values to be used for deriving SWE from SD DEMs, and also to validate SD and SWE estimate outputs.

RPAS-SfM outputs capture the distribution of SD and SWE at a level of detail that is impossible using traditional snow course and weather station data. Individual wind events are capable of greatly altering the distribution of snow. When redistribution of snow takes place where a weather station or snow course is positioned, over and underestimations of SD across an area can occur, however, such anomalies are captured within RPAS-SfM outputs. The ability of RPAS-SfM to estimate snow volume across 50 hectares in a single day offers opportunities to enhance and better validate models used in water monitoring, which could provide increased certainty of snow water volume estimates used for managing community and ecosystem water supply. Likewise, operationalized RPAS-SfM SD surveying could be implemented to increase confidence in flood forecasting, and monitoring of snowpack for hydroelectric generation by extrapolating values across watersheds and regions (Broxton & van Leeuwen, 2020).

Within this study plot, the mean RPAS SD varied considerably from the lower installed weather station, while the upper station reported depths within 0.3 m of the mean (Figure 22). For weather stations being installed primarily to monitor snowpack, the availability of RPAS-SfM SD maps and the SD mean in an area of interest can aid in determining optimal installation sites that can better represent a basin or watershed. Further, having these tools can also aid in positioning weather stations to capture spatial SD variation. In the same way, the positioning of manual snow surveys that are often conducted at weather station sites could be optimized using RPAS-SfM SD maps. As shown in Figures 22 and 23, SD-DEMs produced using RPAS-SfM

techniques provide detailed distribution data which is not shown in manual measurements . Using RPAS-SfM SD maps could be used to position manual snow measurements in locations that are known to consistently contain SD similar to the RPAS-SfM SD mean, and be used to guide the distribution of sample points to capture a distribution of depths across a study plot. RPAS-SfM SD outputs may work to extrapolate SD across a study plot based on previous RPAS-SfM SD surveys, as Broxton & van Leeuwen (2020) did using RPAS-SfM and previous LiDAR data to extrapolate SD.

Chapter 5: Recommendations and Conclusion

5.1 Recommendations

A key recommendation when conducting RPAS-SfM SD surveys in areas with thick ground covering vegetation is to conduct validation surveys on bare earth with no vegetation, such as on roads. This will identify any bias associated with the collection of data or SfM processing that is not associated with vegetation and or complex surface terrain. Validations should also be conducted in vegetated areas, as well as both steep and flat areas to identify any systematic and random errors that may be associated with such features. In this particular study area, roads intersecting the terrain were an ideal location to position transects on, and across. Numerous transects were positioned running across roads, with beginning and ending points in vegetated areas to show how agreement between RPAS-SfM SD estimates and validation measurements varied between such terrain types. To allow more ground points to be identified in SfM processing, snow-off surveys of vegetated terrain should be conducted as soon possible after snowpack ablation has occurred when shrubs will have not yet fully rebounded after being pressed down by the winter snowpack, and annual vegetation growth is still minimal.

In locations where repeat RPAS-SfM SD surveying is planned, the installation of a permanent GCP network is an effective way to save a significant amount of time during field campaigns, and during post processing. During field rover coordinate collections, typically, GNSS units are attached to a monopod and leveled using a simple circular level. Keeping a monopod perfectly level for the required minimum 30 second coordinate collection time, especially when working in the snow, can be very difficult. The ability to quickly screw the GNSS head onto the permanent GCPs worked to insure high DEM accuracy and precision, while

also saving time and effort. When it was clear that the position of the GCPs was static, there was no longer a need to collect GNSS points moving forward. Even in this high snowfall study plot, GCPs remained largely snow free, and only two of 18 were ever completely buried under the snowpack. As recommended by Gindraux et al. (2017), the GCP network was installed so that most areas within the study plot were within 100 m of an individual GCP to minimize DEM error. In addition to the significant time savings, a key advantage of having a GCP network installed is the ability to commence RPAS flights immediately upon arrival at a study plot.

The use of paprika to mark where SD and SWE measurements were collected, and to create temporary GCPs during snow-on surveys, proved to be an efficient way to save a significant amount of time while in the field. The paprika remained highly visible in RPAS imagery, allowing for accurate and quick matching of measurement point locations during post-processing. This method removed the need to collect coordinates at SD and SWE measurement points, and was another significant timesaver. When using this method, particular for creating GCPs, weather conditions must be considered as warm temperatures can cause dissolvable GCPs to become distorted. Further, dissolvable manual measurement markings and GCPs can easily be covered by drifting snow, therefore, if cold unconsolidated snow that may readily drift is present, the use of this method should be carefully evaluated.

As was found in previous studies (Cimoli et al., 2017; Gindraux et al., 2017; Tonkin & Midgley, 2016), when RPAS flights are conducted soon after a recent snowfall, the number of point matches within point clouds, and consequently, the level of precision as well as accuracy of DEMs can be greatly reduced. Waiting at least 24 - 48 hours after a snowfall allows new snow to begin to settle and gain contrast in the process, which can greatly improve end results. Surface

winds can accelerate this process by giving texture to the snow surface, which increases the number of point matches during SfM processing. In the spring when the snow surface becomes textured with melt patterns, forest litter, and dust, a greater number of point matches can be expected.

The time that is required to conduct RPAS flights across a large study plot such as was examined here can make it challenging, or impossible to collect images during the best lighting window of the day (several hours on either side of solar noon). This is especially true during mid-winter and early spring, as was seen in SNOW21:March when shadowing from the low sun angle caused large areas of the output DEM to contain very high error values (Figure 13 & 20). Further, it may not be necessary to survey such a large plot in order to effectively describe the SD and SWE of an area. Sub-sampling could be applied as a means to both save time, and improve mid-winter SfM outputs.

If a large area has been previously surveyed, existing outputs can be used to guide the distribution of sub-sampling plots. Multiple small rectangular plots, or one or more narrow swaths that cover variations in elevation, aspect, and wind exposure could be distributed to cover areas that capture the SD mean and distribution of a study area. However, if doing so, GCP distribution and the typically increased error levels found near DEM edges must be considered; RPAS imagery should be collected 50 -100 beyond the desired sample area so that DEM edges can be trimmed off. As detailed in section 2.4.3, to achieve sub-decimetre DEM accuracy, GCPs should be evenly distributed across flight plots so that no area is more than 100 m from a GCP, while at least 4 GCPs should be used (Tonkin & Midgley, 2016).

Without previous SD maps to use as guidance, among other parameters, sub-sampling strategies should take into account solar aspect, elevation, wind exposure, and prominent shadowing, all of which can affect SD across a landscape. Existing multiple linear regression and multivariate SD models could work to help guide the placement of RPAS sub-sample plots to capture the mean and distribution of SD across a watershed (Jenicek et al., 2018; Grunewald et al., 2013). Similarly, RPAS-SfM SD outputs could be used to train and validate SD models that are used to estimate SD distribution at a watershed level.

5.2 Future Research

To date, the general focus of RPAS-SfM SD research has been validation across varying terrain (Bühler et al., 2017; Cimoli et al., 2017; De Michele, et al., 2016; Harder et al., 2016; Lendzioch et al., 2019). The current, and previous studies show that these techniques can be applied across a variety of landscape types. Moving forward, there will be great value in exploring how RPAS-SfM SD outputs can be used for extrapolating total water stored as snow at watershed, or regional levels. To that point, as described above, Broxton & van Leeuwen, (2020) have successfully combined previous LiDAR outputs with sample area RPAS-SfM SD outputs to extrapolate snow across spatially broad areas. This approach of using previous outputs to base extrapolation on could also be applied to RPAS-SfM outputs by initially conducting spatially broad surveys throughout a snow season, then doing smaller samples later. Another application to explore is the use RPAS-SfM SD mapping for improving the positioning of weather stations and long-term manual snow sampling plots.

Using the technology that exists today, RPAS-SfM SD estimations in areas with tall and thick ground covering vegetation will always have a certain level of uncertainty, which manifests

primarily as a negative bias; adding positive offsets to DEMs where a consistent negative bias caused by rebounding vegetation exists is a practical and simple way to improve overall certainty of results. More research into this method would be useful to increase the precision of offsets across complex study plots. Where appropriate, strips of vegetation within thickly vegetated plots could be cleared, from which better precision offsets may be determined. If a new snow research site is to be established where a large disturbances has occurred such as a forest fire, or a forest harvesting cutblock, collecting RPAS-SfM bare earth data immediately after the disturbance occurs, and before regrowth has begun could work well to monitor SD in such an area.

5.3 Conclusion

Throughout the world, the shifting climate and changes to land cover are altering snow hydrology. In regions where population growth is increasing pressure on already strained water resources, having a more accurate knowledge of the volume of water stored as snow has never been more important. This study examined the use of RPAS-SfM technology to estimate and map SD and SWE in a spatially broad, complex, recently logged, mid-elevation study plot that contains thick ground covering perennial vegetation. Prior to this study, RPAS-SfM SD mapping had not been attempted in such terrain. This research expands on methods developed in previous studies, while also exploring new methods to improve efficiency and accuracy when conducting RPAS-SfM SD surveys in complex vegetated terrain. Total stored water estimates were calculated from produced SD-DEMs and manual snow density measurements. Further, prior to this study, no published accounts of RPAS-SfM SD surveying in British Columbia or elsewhere on the west coast of North America existed, while literature of surveying complex terrain with

thick vegetation remains limited (Gaffey & Bhardwaj, 2020; Harder et al., 2016; Jagt et al., 2015; Lendzioch et al., 2016).

The collection of overlapping RGB photo imagery of snow surface and bare earth conditions was conducted using a consumer grade RPAS, while DEMs were created in *Agisoft PhotoScan Pro 1.5.2* SfM photogrammetry software. SD was estimated by subtracting a bare earth DEM from snow surface DEMs, while mean snow density for each field campaign was used to derive SWE across the study area. Estimated SD and SWE values were validated using manually collected SD and SWE measurements. High precision RTK GNSS coordinates were collected at permanently installed GCPs. These permanent GCPs greatly reduced the amount of time needed in the field. Without the need to distribute temporary GCPs before commencing flights, the installed permanent GCP network allowed field crews to begin surveying promptly upon arrival at the study plot. Permanent GCPs also served as ideal platforms to collect GNSS points, and situate SD and SWE validation transects from. Further, having a permanent GCP network in place and RTK GNSS point collection and corrections already complete allowed for preliminary snow-on survey results to be completed within 24 hours upon returning from the field. Paprika was used as a highly visible, low-cost, non-toxic medium to mark manual measurement points, removing the need to collect GNSS points at validation locations, which saved a substantial amount of time both in the field, and during post-processing. When snowmelt or blowing snow was not a concern, paprika was also found to be useful for creating additional GCPs by applying it to the snow surface using a stencil.

Three of the four snow-on surveys conducted returned overall good results, while a single survey conducted in early March was problematic due to heavy shadowing and inconsistent

lighting conditions. In vegetation free areas, RPAS-SfM SD surveying returned SD estimates with error values comparable to previous studies noted above, however, levels of error varied considerably throughout the study plot. Perfect matches between manually measured individual SD points and RPAS-SfM SD estimates were found on roads and other unvegetated areas, while in areas where tall shrub growth was present, differences of over 0.50 m existed. RMSE ranged from 0.08 m on road sections under ideal lighting and snow surface conditions, and up to 0.56 m in vegetated off-road areas when fresh snow was present, and lighting conditions were poor. In these off-road areas, RMSE initially ranged from 0.36 m to 0.59 m, however, the bias correction was effective for dealing with underestimations of SD values caused by thick perennial vegetation. The application of positive vertical offsets to off-road sections reduced RMSE by up to 0.27 m, resulting in best case RMSE of 0.18 m in such areas. SWE values derived from SD DEMs had RMSE ranging from 0.04 m on road section, and up to 0.24 m in vegetated areas.

In this study, as noted in Gindraux et al., (2017) the importance of conducting RPAS SD surveys several days after fresh snow has fallen was reconfirmed here. Increased error levels were found during both surveys that were conducted within 24 hours from when snowfall had occurred. Conducting RPAS-SfM snow surveys in the vicinity of tall forest stands, especially in the winter when long shadows are cast due to low sun angle, can result in very high error values in areas of deep shadowing as was found during SNOW21:March. However, despite there being areas were high error occurred, useful results outside of shadowed areas did exist. Of the four snow-surface surveys conducted during this study, best accuracy DEMs and RPAS-SfM SD estimates were produced from images collected in May when sun angle was high, no new snow had fallen in some time, and snow surface conditions consisted of well consolidated snow, that

included the presence of forest litter. When planning RPAS-SfM surveys in mid-latitude regions, surveys should be planned in open areas away from mountain, ridges or forests that may cast shadows, especially earlier in the snow season when the sun angle is low, and long shadows are cast from adjacent forests and ridges. While accuracy of surveys conducted into the spring are likely to be better due to superior illumination and increased likelihood of ideal snow surface conditions, it is still possible to obtain useful results outside of shadowed areas during the winter.

Spatially broad SD validation sampling is important in confirming the accuracy of RPAS-SfM outputs throughout a study plot. When deriving SWE from SD-RPAS, manual SWE measurements should be widespread across the study area to ensure that the mean density values used to derive SWE from SD DEMs are as representative and accurate as possible. This is especially important in colder drier climates where the density of snow can range from 30 kg/m^3 for new snow that falls under calm conditions, and up to 300 kg/m^3 in areas where the snow is wind packed (McClung & Schaerer, 2006). In vegetated areas where offsets are to be used, it is important to conduct validation measurements widely throughout the study plot in order to calculate effective and accurate offset values. Further, when possible, it is important to collect validations on road, or other vegetation-free areas to determine bias that may exist in such areas, and to aid in determining offset values. If this study was to be done again, a more systematic snow validation method would be employed, as well as more robust surface vegetation measurements.

As highlighted in previous studies (Gaffey & Bhardwaj, 2020; Harder et al., 2020; Harder et al., 2016; Jagt et al., 2015; Lendzioch et al., 2016), perennial vegetation was found to introduce a significant negative bias to RPAS SD estimates. The problem of perennial ground

covering vegetation introducing significant negative bias to results remains a challenge in this field, however, the results of this study offer approaches that can improve accuracy and certainty of results in such areas. New methods introduced here offer ways to improve efficiency and reduce the amount of time needed to conduct RPAS-SfM field surveys, as well as reducing the number of field technicians needed during most field campaigns.

Appendix

As part of a pilot study, a modified version of the above described sampling pattern was analyzed. Four 24 x 24 m plots were completed, with the same 1 m SD and 3 m SWE sampling intervals used in Jost et al. (2007). Analysis of the data collected showed that in open areas, transect means are virtually unchanged when only every second SD measurement is included in the analysis; with this adjustment applied, change to the transect SD mean of 1.86 m was negligible, and smaller than the sampling precision of 0.01 m (Table 7). Similarly, small changes were observed when reducing the number of SWE measurements; including only 3 of 9 measurements on a singular transect altered the mean by 7% in this analysis. In treed areas where the snowpack has more variation, reducing the number of sample points caused greater shifts to the mean of transects and plots. In a transect with a mean of 1.17 m, reducing the number of SD samples by half to 2 m intervals resulted in a mean of 1.14 m. When SWE measurements were reduced by half, the mean shifted by 3.36%, with a reduction to five sample points resulting in a 13.79% shift.

Table 7. Snow depth mean comparison between all points, and with the half points removed.

	Cutblock W-E		Cutblock S-N		Forest W-E		Forest S-N	
n =	25	13	25	13	25	13	25	13
Average Snow Depth (m)	1.17	1.16	1.17	1.14	1.83	1.86	1.82	1.81
Change in Average SD (m)	0.012		0.029		0.036		0.014	

References

Adams, M. S., Bühler, Y., & Fromm, R. (2017). multitemporal accuracy and precision assessment of unmanned aerial system photogrammetry for slope-scale snow depth maps in alpine terrain. *Pure and Applied Geophysics*. https://doi.org/10.1007/s00024-017-1748-y

Agisoft. (2022). Agisoft metashape user manual professional edition, version 1.8. (2022).

Avanzi, F., Bianchi, A., Cina, A., De Michele, C., Maschio, P., Pagliari, D., … Rossi, L. (2018). Centimetric accuracy in snow depth using unmanned aerial system photogrammetry and a multistation. *Remote Sensing*, *10*(5), 765. https://doi.org/10.3390/rs10050765

Bhardwaj, A., Sam, L., Akanksha, Martín-Torres, F. J., & Kumar, R. (2016). UAVs as remote sensing platform in glaciology: present applications and future prospects. *Remote Sensing of Environment*, *175*, 196–204. https://doi.org/10.1016/J.RSE.2015.12.029

Bongio, M., Arslan, A. N., Tanis, C. M., & Michele, C. De. (2021). Snow depth time series retrieval by time-lapse photography: Finnish and Italian case studies. *The Cryosphere*, *15*(1), 369–387. https://doi.org/10.5194/TC-15-369-2021

Broxton, P. D., & van Leeuwen, W. J. D. (2020). Structure from motion of multi-angle rpas imagery complements larger-scale airborne lidar data for cost-effective snow monitoring in mountain forests. *Remote Sensing 2020, Vol. 12, Page 2311*, *12*(14), 2311. https://doi.org/10.3390/RS12142311

Bühler, Y., Adams, M. S., Bösch, R., & Stoffel, A. (2016). Mapping snow depth in alpine terrain with unmanned aerial systems (UASs): potential and limitations. *The Cryosphere*, *10*(3), 1075–1088. https://doi.org/10.5194/tc-10-1075-2016

Bühler, Y., Adams, M. S., Stoffel, A., & Boesch, R. (2017). Photogrammetric reconstruction of

homogenous snow surfaces in alpine terrain applying near-infrared UAS imagery. *International Journal of Remote Sensing*, *38*(8–10), 3135–3158. https://doi.org/10.1080/01431161.2016.1275060

CHRL. (n.d.). High elevation weather station network. Retrieved September 10, 2021, from http://www.viu-hydromet-wx.ca/high-elevation-weather-station-network/

Cimoli, E., Marcer, M., Vandecrux, B., Bøggild, C. E., Williams, G., & Simonsen, S. B. (2017). Application of low-cost uass and digital photogrammetry for high-resolution snow depth mapping in the Arctic. *Remote Sensing*, *9*(11), 1144. https://doi.org/10.3390/rs9111144

Cline, D. (1993). Measuring alpine snow depths by digital photogrammetry. part 1. conjugate point identification | western snow conference. Retrieved April 13, 2020, from https://westernsnowconference.org/node/511

Collados-Lara, A.-J., Pardo-Igúzquiza, E., & David Pulido-Velazquez, . (2019). Optimal design of snow stake networks to estimate snow depth in an alpine mountain range. *Hydrological Processes*, *34*, 82-92. https://doi.org/10.1002/hyp.13574

Collados-Lara, A.-J., Pardo-Igúzquiza, E., & Pulido-Velazquez, D. (2017). Spatiotemporal estimation of snow depth using point data from snow stakes, digital terrain models, and satellite data. *Hydrological Processes*, *31*(10), 1966–1982. https://doi.org/10.1002/hyp.11165

Colomina, I., & Molina, P. (2014). Unmanned aerial systems for photogrammetry and remote sensing: A review. *ISPRS Journal of Photogrammetry and Remote Sensing*, *92*, 79–97. https://doi.org/10.1016/J.ISPRSJPRS.2014.02.013

Cunliffe, A. M., Brazier, R. E., & Anderson, K. (2016). Ultra-fine grain landscape-scale

quantification of dryland vegetation structure with drone-acquired structure-from-motion photogrammetry. *Remote Sensing of Environment*, *183*, 129–143. https://doi.org/10.1016/J.RSE.2016.05.019

De Michele, C., Avanzi, F., Passoni, D., Barzaghi, R., Pinto, L., Dosso, P., … Della Vedova, G. (2016). Using a fixed-wing UAS to map snow depth distribution: an evaluation at peak accumulation. *The Cryosphere*, *10*(2), 511–522. https://doi.org/10.5194/tc-10-511-2016

Deems, J. S., Painter, T. H., & Finnegan, D. C. (2013). Lidar measurement of snow depth: a review. *Journal of Glaciology*, *59*(215), 467–479. https://doi.org/10.3189/2013JoG12J154

DJI. (2021). Phantom 4 pro - product information - dji. Retrieved from https://www.dji.com/ca/phantom-4-pro/info#specs

Donahue, B.; Wentzel, J.; Berg, R. (2013). *Guidelines for rtk/rtn gnss surveying in canada ministry of transportation ministère des transports*.

Easy, D. M. (2021). Map pilot pro. Retrieved from https://dronesmadeeasy.com/map-pilot

Ely, J. C., Graham, C., Barr, I. D., Rea, B. R., Spagnolo, M., & Evans, J. (2017). Using uav acquired photography and structure from motion techniques for studying glacier landforms: application to the glacial flutes at Isfallsglaciären. *Earth Surface Processes and Landforms*, *42*(6), 877–888. https://doi.org/10.1002/esp.4044

ESRI (2022). The image classification wizard. Retrieved from https://pro.arcgis.com/en/pro-app/2.7/help/analysis/image-analyst/the-image-classification-wizard.htm

Fernández, T., Pérez, J., Cardenal, J., Gómez, J., Colomo, C., Delgado, J., … Delgado, J. (2016). Analysis of landslide evolution affecting olive groves using uav and photogrammetric techniques. *Remote Sensing*, *8*(10), 837. https://doi.org/10.3390/rs8100837

Ferraz, A., Saatchi, S., Bormann, K., Painter, T., Ferraz, A., Saatchi, S., … Painter, T. H. (2018). Fusion of nasa airborne snow observatory (aso) lidar time series over mountain forest landscapes. *Remote Sensing*, *10*(2), 164. https://doi.org/10.3390/rs10020164

Fraser, B., Congalton, R., Fraser, B. T., & Congalton, R. G. (2018). Issues in unmanned aerial systems (uas) data collection of complex forest environments. *Remote Sensing*, *10*(6), 908. https://doi.org/10.3390/rs10060908

Gaffey, C., & Bhardwaj, A. (2020). applications of unmanned aerial vehicles in cryosphere: latest advances and prospects. *Remote Sensing*, *12*(6), 948. https://doi.org/10.3390/RS12060948

Gindraux, S., Boesch, R., & Farinotti, D. (2017). Accuracy assessment of digital surface models from unmanned aerial vehicles' imagery on glaciers. *Remote Sensing*, *9*(2), 186. https://doi.org/10.3390/rs9020186

Giordan, D., Hayakawa, Y., Nex, F., Remondino, F., & Tarolli, P. (2018). Review article: the use of remotely piloted aircraft systems (rpas) for natural hazards monitoring and management. *Hazards Earth Syst. Sci*, *18*, 1079–1096. https://doi.org/10.5194/nhess-18-1079-2018

Girod, L., & Filhol, S. (2020). Absolute coregistration and doming correction in adverse conditions, or how to retrieve snow depth from drone flights. *ISPRS Annals of the Photogrammetry, Remote Sensing and Spatial Information Sciences*, *V-3–2020*(3), 375–379. https://doi.org/10.5194/ISPRS-ANNALS-V-3-2020-375-2020

Grunewald, T., Stotter, J., Pomeroy, J., Dadic, R., Moreno Banos, I., Marturia, M., … Lehning, M. (2013). Statistical modelling of the snow depth distribution in open alpine terrain. *Hydrology and Earth System Sciences, 17*(8), 3005-3021.

Guerra-Hernández, J., González-Ferreiro, E., Monleón, V., Faias, S., Tomé, M., Díaz-Varela, R., … Díaz-Varela, R. A. (2017). Use of multi-temporal uav-derived imagery for estimating individual tree growth in pinus pinea stands. *Forests*, *8*(8), 300. https://doi.org/10.3390/f8080300

Harder, P., Pomeroy, J. W., Helgason. (2017). Local-scale advection of sensible and latent heat during snowmelt. *Geophysical Research Letters. 44*(19), 9769-9777. https://doi.org/10.1002/2017GL074394

Harder, P., Pomeroy, & J. W., Helgason. (2020). Improving sub-canopy snow depth mapping with unmanned aerial vehicles: lidar versus structure-from-motion techniques. *The Cryosphere*, *14*(6), 1919–1935. https://doi.org/10.5194/TC-14-1919-2020

Harder, P, Schirmer, M., Pomeroy, J., & Helgason, W. (2016). Accuracy of snow depth estimation in mountain and prairie environments by an unmanned aerial vehicle. *The Cryosphere*, *10*(6), 2559–2571. https://doi.org/10.5194/tc-10-2559-2016

Harpold, A. A., Guo, Q., Molotch, N., Brooks, P. D., Bales, R., Fernandez-Diaz, J. C., … Lucas, R. (2014). LiDAR-derived snowpack data sets from mixed conifer forests across the Western United States. *Water Resources Research*, *50*(3), 2749–2755. https://doi.org/10.1002/2013WR013935

Hugenholtz, C. H., Whitehead, K., Brown, O. W., Barchyn, T. E., Moorman, B. J., Leclair, A., … Hamilton, T. (2013). Geomorphological mapping with a small unmanned aircraft system (suas): feature detection and accuracy assessment of a photogrammetrically-derived digital terrain model. *Geomor*, *194*. https://doi.org/10.1016/j.geomorph.2013.03.023

Izumida, A., Uchiyama, S., & Sugai, T. (2017). Application of uav-sfm photogrammetry and

aerial lidar to a disastrous flood: repeated topographic measurement of a newly formed crevasse splay of the Kinu River, central Japan. *Hazards Earth Syst. Sci*, *17*, 1505–1519. https://doi.org/10.5194/nhess-17-1505-2017

Jagt, B., Lucieer, A., Wallace, L., Turner, D., & Durand, M. (2015). Snow depth retrieval with uas using photogrammetric techniques. *Geosciences*, *5*(3), 264–285. https://doi.org/10.3390/geosciences5030264

James, M. R., & Robson, S. (2014). Mitigating systematic error in topographic models derived from UAV and ground-based image networks. *Earth Surface Processes and Landforms*, *39*(10), 1413–1420. https://doi.org/10.1002/esp.3609

Jenichek, M., Pevna, H., & Matejka, O. (2018). Canopy structure and topography effects on snow distribution at a catchment scale: *Application of multivariate approaches. Journal of Hydrology and Hydromechanics*, *66*(1), 43-54. http://dx.doi.org/10.1515/johh-2017-0027

Jost, G., Weiler, M., Gluns, D. R., & Alila, Y. (2007). The influence of forest and topography on snow accumulation and melt at the watershed-scale. *Journal of Hydrology*, *347*(1–2), 101–115. https://doi.org/10.1016/j.jhydrol.2007.09.006

Lendzioch, T., Langhammer, J., & Jenicek, M. (2016). tracking forest and open area effects on snow accumulation by unmanned aerial vehicle photogrammetry. *ISPRS - International Archives of the Photogrammetry, Remote Sensing and Spatial Information Sciences*, *XLI-B1*, 917–923. https://doi.org/10.5194/isprs-archives-XLI-B1-917-2016

Lendzioch, Theodora, Langhammer, J., & Jenicek, M. (2019). Estimating snow depth and leaf area index based on uav digital photogrammetry. *Sensors (Basel, Switzerland)*, *19*(5). https://doi.org/10.3390/S19051027

Lucieer, A., Jong, S. M. de, & Turner, D. (2014). Mapping landslide displacements using structure from motion (sfm) and image correlation of multi-temporal UAV photography. *Progress in Physical Geography*, *38*(1), 97–116. https://doi.org/10.1177/0309133313515293

Marti, R., Gascoin, S., Berthier, E., de Pinel, M., Houet, T., & Laffly, D. (2016). Mapping snow depth in open alpine terrain from stereo satellite imagery. *The Cryosphere*, *10*(4), 1361–1380. https://doi.org/10.5194/tc-10-1361-2016

McClung, D., & Schaerer, P. A. (2006). The avalanche handbook. Mountaineers Books.

Meidinger, D. V, & Pojar, J. (1991). Ecosystems of British Columbia. BC Ministry of Forests. Retrieved from https://www.for.gov.bc.ca/hfd/pubs/Docs/Srs/Srs06.pdf

Miziński, B., & Niedzielski, T. (2017). Fully-automated estimation of snow depth in near real time with the use of unmanned aerial vehicles without utilizing ground control points. *Cold Regions Science and Technology*, *138*, 63–72. https://doi.org/10.1016/J.COLDREGIONS.2017.03.006

Natural Resources Canada. (2013). Guidelines for rtk/rtn gnss surveying in Canada. Retrieved from https://www.nrcan.gc.ca/sites/www.nrcan.gc.ca/files/earthsciences/pdf/Canada-RTK-UserGuide-v1_1-EN.pdf

Niedzielski, T., Szymanowski, M., Mizinski, B., Spallek, W., Witek-Kasprzak, M., Slopek, J., …. Leszczynski, L. (2019). Estimating snow water equivalent using unmanned aerial vehicles for determining snow-melt runof. *Journel of Hydrology, 578.* https://doi.org/10.1016/j.jhydrol.2019.124046.

Nolan, M., Larsen, C., & Sturm, M. (2015). Mapping snow depth from manned aircraft on

landscape scales at centimeter resolution using structure-from-motion photogrammetry. *The Cryosphere*, *9*(4), 1445–1463. https://doi.org/10.5194/tc-9-1445-2015

Pacific Climate Impacts Consortium. (2021). Seasonal anomaly maps. Retrieved October 28, 2021, from https://www.pacificclimate.org/analysis-tools/seasonal-anomaly-maps

Province of British Columbia. (n.d.). Wildfire averages. Retrieved January 10, 2022, from https://www2.gov.bc.ca/gov/content/safety/wildfire-status/about-bcws/wildfire-statistics/wildfire-averages

Raleigh, M. S., & Small, E. E. (2017). Snowpack density modeling is the primary source of uncertainty when mapping basin-wide SWE with lidar. *Geophysical Research Letters*, *44*, 3700–3709. https://doi.org/10.1002/2016GL071999

Revuelto, J., Alonso-Gonzalez, E., Vidaller-Gayan, I., Lacroix, E., Izagirre, E., Rodríguez-López, G., & López-Moreno, J. I. (2021). Intercomparison of uav platforms for mapping snow depth distribution in complex alpine terrain. *Cold Regions Science and Technology*, *190*, 103344. https://doi.org/10.1016/J.COLDREGIONS.2021.103344

Revuelto, J., López-Moreno, J. I., & Alonso-González, E. (2021). Light and shadow in mapping alpine snowpack with unmanned aerial vehicles in the absence of ground control points. *Water Resources Research*, *57*(6), e2020WR028980. https://doi.org/10.1029/2020WR028980

Ryan, J. C., Hubbard, A. L., Box, J. E., Todd, J., Christoffersen, P., Carr, J. R., … Snooke, N. (2015). UAV photogrammetry and structure from motion to assess calving dynamics at Store Glacier, a large outlet draining the Greenland ice sheet. *The Cryosphere*, *9*(1), 1–11. https://doi.org/10.5194/tc-9-1-2015

Snow Survey Data - Province of British Columbia. (n.d.). Retrieved August 30, 2021, from https://www2.gov.bc.ca/gov/content/environment/air-land-water/water/water-science-data/water-data-tools/snow-survey-data

Solbø, S., & Storvold, R. (2013). mapping Svalbard glaciers with the cryowing uas. *International Archives of the Photogrammertry, Remote Scensing and Spatial Information Sciences*. Retrieved from http://uas.norut.no.

Sturm, M., Taras, B., Liston, G. E., Derksen, C., Jonas, T., & Lea, J. (2010). estimating snow water equivalent using snow depth data and climate classes. *Journal of Hydrometeorology*, *11*(6), 1380–1394. https://doi.org/10.1175/2010JHM1202.1

Tonkin, T., & Midgley, N. (2016a). ground-control networks for image based surface reconstruction: an investigation of optimum survey designs using uav derived imagery and structure-from-motion photogrammetry. *Remote Sensing*, *8*(9), 786. https://doi.org/10.3390/rs8090786

Tonkin, T., & Midgley, N. (2016b). ground-control networks for image based surface reconstruction: an investigation of optimum survey designs using uav derived imagery and structure-from-motion photogrammetry. *Remote Sensing*, *8*(9), 786. https://doi.org/10.3390/rs8090786

Vore, M. E., Déry, S. J., Hou, Y., & Wei, X. (2020). Climatic influences on forest fire and mountain pine beetle outbreaks and resulting runoff effects in large watersheds in British Columbia, Canada. *Hydrological Processes*, *34*(24), 4560–4575. https://doi.org/10.1002/HYP.13908

Wainwright, H. M., Liljedahl, A. K., Dafflon, B., Ulrich, C., Peterson, J. E., Gusmeroli, A., &

Hubbard, S. S. (2017). Mapping snow depth within a tundra ecosystem using multiscale observations and Bayesian methods. *The Cryosphere*, *11*(2), 857–875. https://doi.org/10.5194/tc-11-857-2017

Wang, T., Hamann, A., Spittlehouse, D., & Carroll, C. (2016). Locally downscaled and spatially customizable climate data for historical and future periods for North America. *PLoS ONE*, *11*(6). https://doi.org/10.1371/JOURNAL.PONE.0156720

Whitehead, K., & Hugenholtz, C. H. (2014). remote sensing of the environment with small unmanned aircraft systems (uass), part 1: a review of progress and challenges. *Journal of Unmanned Aircraft Systems*, *02*(03), 69–85. Retrieved from http://people.ucalgary.ca/~kwhitehe/Review_part1_draft.pdf

Whitehead, K., Hugenholtz, C. H., Myshak, S., Brown, O., Leclair, A., Tamminga, A., … Eaton, B. (2014). remote sensing of the environment with small unmanned aircraft systems (uass), part 2: scientific and commercial applications 1. *J. Unmanned Veh. Syst. J. Unmanned Veh. Sys*, *212*(18), 86–102. Retrieved from http://www.nrcresearchpress.com/doi/pdfplus/10.1139/juvs-2014-0007

Wigmore, O., & Mark, B. (2017). Monitoring tropical debris-covered glacier dynamics from high-resolution unmanned aerial vehicle photogrammetry, Cordillera Blanca, Peru. *The Cryosphere*, *11*. https://doi.org/10.5194/tc-11-2463-2017

Yildiz, S., Akyurek, Z., & Binley, A. (2021). Quantifying snow water equivalent using terrestrial ground penetrating radar and unmanned aerial vehicle photogrammetry. *Hydrological Processes*, *35*(5), e14190. https://doi.org/10.1002/HYP.14190